REMOTE THERMOMETRY AND MICROTHERMOMETRY

Tesis presentada por
MC. Juan Arturo Aranda Ruiz

Como requisito para obtener el grado de Doctor en Ciencias
(Óptica)

León, Gto. Enero del 2008

Dedicatoria

Dedico este trabajo a mi esposa Silvia Angel O., quien durante este tiempo me apoyo y soporto, que junto con mis hijos Lizeth, Melissa y Juan Arturo fueron mi inspiración y motivación a continuar.

Agradecimiento

Al Dr. Gonzalo Páez P. ya que gracias a su apoyo, guía y paciencia fue posible la realización de este trabajo; al igual que la contribución indispensable de la Dra. Marija Strojnik en la conclusión de este esfuerzo. También a los compañeros de grupo Eduardo, Claudio, Paulino, Camille, Max, Enoch Mariana y J. Carlos por sus comentarios y consejos. Al personal de formación académica, especialmente a Guille por su empeño y dedicación.

Table of contents

List of Figures

Figures Chapter 3

Figures Chapter 4

List of Tables

Introduction

1. Background

Remote sensing systems have been applied in a many situations , chiefly in situations where they do not interfere in the process that they monitor and it is not necessary to destroy the object, which is monitored. Among the non-destructive remote sensing methods, the monitoring in the infrared spectral region is the most popular. This happens due the atmosphere's characteristics and non-interference with the visible radiation.

Herschel discovered infrared radiation in 1800, by passing sunligth through a prism and holding a thermometer just beyond the red end of the visible spectrum. He was astonished when it showed a higher temperature than the obtained from the visible spectrum. Further experimentation led to Herschel's conclusion that there must be an invisible form of light beyond the visible spectrum.

This invisible radiation for humans imply that the IR detector must act as a transducer between the image in the infrared and visible (Paez, Strojnik; Sandoval; Vacas-Jacques [2002]). (Paez; Alfaro, Strojnik [2006]). (Paez, Strojnik [2006]. (Strojnik [2007])).

Monitoring the environment on the earth has become an everyday issue to clarify risks from global warming and natural hazards. Also tracking the condition of forests, fisheries, water and other resources. The ability to follow retreating polar ice and shifting patterns of drought, rainfall and other environmental changes (Skrbek 2000). We are interested in a range of temperature of the objects at environmental temperature.

Monitoring of the Earth resources assumes the temperature of the earth, water or vegetation that covers it at about *300* K. Small changes observed in the infrared band indicate different vegetation coverage. Also it may indicate an early warning signal due to the onset of a disease or the presence of a stress due to the lack of water caused by draught (Aldaklheel [2000]).

We are interested in remotely monitoring large crop areas [1], Fig 1. It may be, for example, a crop of *agave azul*, a plant that takes several years before bearing fruit. Once a plant is found to be infected, it is destroyed. Due to his lengthy maturation cycle (about 10 years), the economic losses are minimized upon early disease identification.

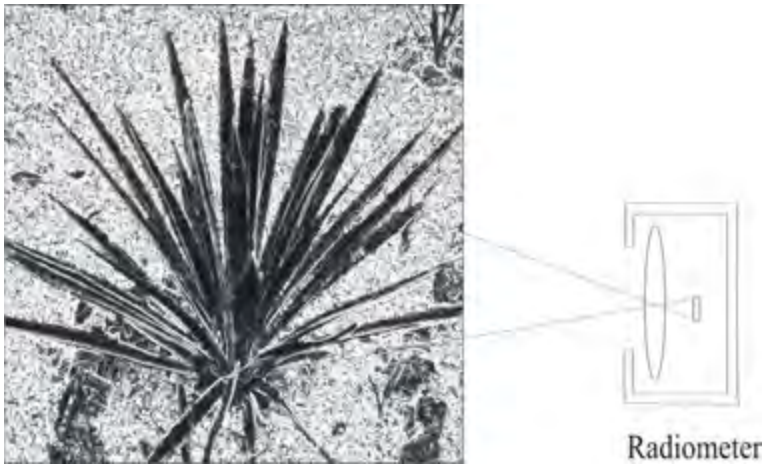

Fig. 1. The plant is remotely monitored. At the close approach, the plant fills the radiometer field-of-view

The changed appearance of the disease-infected plant may, in principle be used to diagnose its state of health and to monitor its progress toward the production of healthy fruit. However , it is well known that the human inspection is not very reliable: humans do not distinguish between small spectral differences of a specific plant on a consecutive

observations. This is due to poor ability of humans to separate color nuances, our inadequate memory, and the absence of absolute internal calibration standards. A machine inspection is significantly superior due to its repeatability, memory and ease of calibration. Monitoring in the IR band region is preferable to that in the visible, because the daylight conditions introduce a significant amount of noise and variability in the measurements.

Let us consider the monitoring scenario, illustrated in Fig. 2. A radiometer operating in the IR spectral region is mounted on a vehicle that passes between two rows of plants. Its field of view may be quite small so that even a small plant fills it. Later on when a plant has grown larger, only a selected horizontal section of a plant is monitored. During the successive passes τ times apart, the detected incidance is recorded. Assuming that the radiometer is calibrated, the only incidance change between the plant with coordinates *(i,j)* goes between E(*i, j, τ)* and E(*i, j, τ+1)* it is that due to the disease symptoms. We are interested in recording the *detected contrast*, defined as the difference in the detected incidance from a healthy and unhealthy plant. We monitor a plant *(i, j)* which from time *t=0* to time $t=K\tau$ to check for healthy.

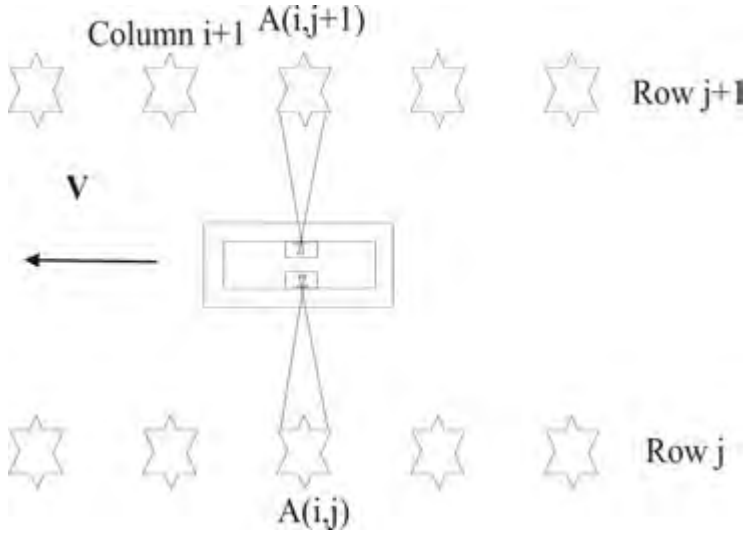

Fig. 2. Monitoring the plant *(i, j)*on the nth pass. A radiometer is mounted on the vehicle passing between two rows of plants.

Thus, its detected incidance is unchanged upon repeated observations. Then, at time $t=K\tau$ the plant starts developing and, consequently, displaying disease symptoms. The infection of a plant with disease modifies its emissivity, its temperature, and the change of emissivity with temperature [2,3,4] (Paez, Strojnik [1997])..

The contribution of the temperature-dependent emissivity to the temperature-dependent gray-body incidence detected in a wavelength interval is shown to be significant, (Paez, Strojnik [1998]). The infection of vegetation with a disease will modify its emissivity, its change of emissivity with temperature, and its temperature.

For remote crop monitoring the quantum detector is more sensitive to the changes in contrast than the thermal detector, (Paez, Strojnik [1999]).

2. Methodology and objectives

In chapter one we reviewed de concepts to asses remote sensing systems and the typical errors that can mislead the measurements, at the chapter two we review the figures of merit from the ideal thermal and quantum detectors and the incidance from a gray body detected in a wavelength interval. We apply the result to a tungsten lamp. At chapter three we will perform the theoretical comparison between the detected thermal contrast measured with a quantum and a thermal detector for an earth based remote monitoring at room temperature process. At chapter four we determine the temperature distribution along a short line with continuous two wavelength thermometry on a micro surface element of the coiled coil whit a spectrometer.

References

[1] J.R. Schott, Remote Sensing: The image Chain Approach, first ed., Oxford University Press, New York, [1997]

[2] O. Staaf, C.G. Ribbing, S.K. Andersson, Temperature dependence of band emittance for nongray bodies, Appl. Opt. 35 (31) (1996) 6120-6125.

[3] G. Paez, M.S. Scholl, Thermal contrast detected with a thermal detector, Infrared Phys. Technol. 40 (1999) 109-116.

[4] G. Paez, M.S. Scholl, Thermal contrast detected with a quantum detector, Infrared Phys. Technol. 40 (1999) 261-265.

Chapter 1

Radiation thermometry

1.1 Introduction

Objects with a temperature greater than 0 K emit electromagnetic radiation. The distribution of the power emission in the electromagnetic spectrum is a function of its temperature. Ideal black bodies obey the Planck's law, but the real bodies emit radiation with a slight modification to this law. To asses the temperature of an object in base of its emitted radiation, we have to take in account the wavelength interval, the transmission path from the object to the sensor, the environment temperature, the fluorescence, the kind of source, such as Lambertian radiators and if there is another source of radiation that can mislead the evaluation of the acquired data. In this chapter we are going to review these concepts, and any factor that can mislead the evaluation of the data.

1.2 Blackbodies and blackbody radiation

The radiation is emitted by hot objects in a wide range of wavelengths of the electromagnetic spectrum. For objects at temperatures of practical interest, most of the radiation lies at the infrared and visible portions of the spectrum [1]. A graphical description of the distribution of thermal radiation is shown in Fig. (1.1)

The spectral radiance plotted on the vertical axis of Fig. (1.1) is a measure of the amount of energy per unit time emitted by an object in a specific direction in a given bandwidth. The horizontal scale describes the wavelengths at which the radiation is emitted. The visible portion of the spectrum is also marked, with the violet end of the visible spectrum at 0.4 μm and the red end at 0.7 μm. Radiation at wavelengths shorter than 0.4 μm is described as ultraviolet (above violet) or UV, while radiation at wavelengths longer than 0.7 μm is described as infrared (below red) or IR.

We can see from Fig. 1 that for objects with a temperature about lower than 500 °C (~800 K) most of the radiation is in the invisible infrared region. As the temperature increases, the radiance curves of Fig. 1.1 begin to edge into the red end of the visible spectrum, we see objects as red hot. As the temperature is further increased, the maximum of the emission spectrum moves closer to the visible portion and we see objects with the perceived colors shown in table 1.1. At temperatures above 1500°C to 1800 °C, objects become so bright that our eyes have difficulty to accurately and comfortably discerning the color.

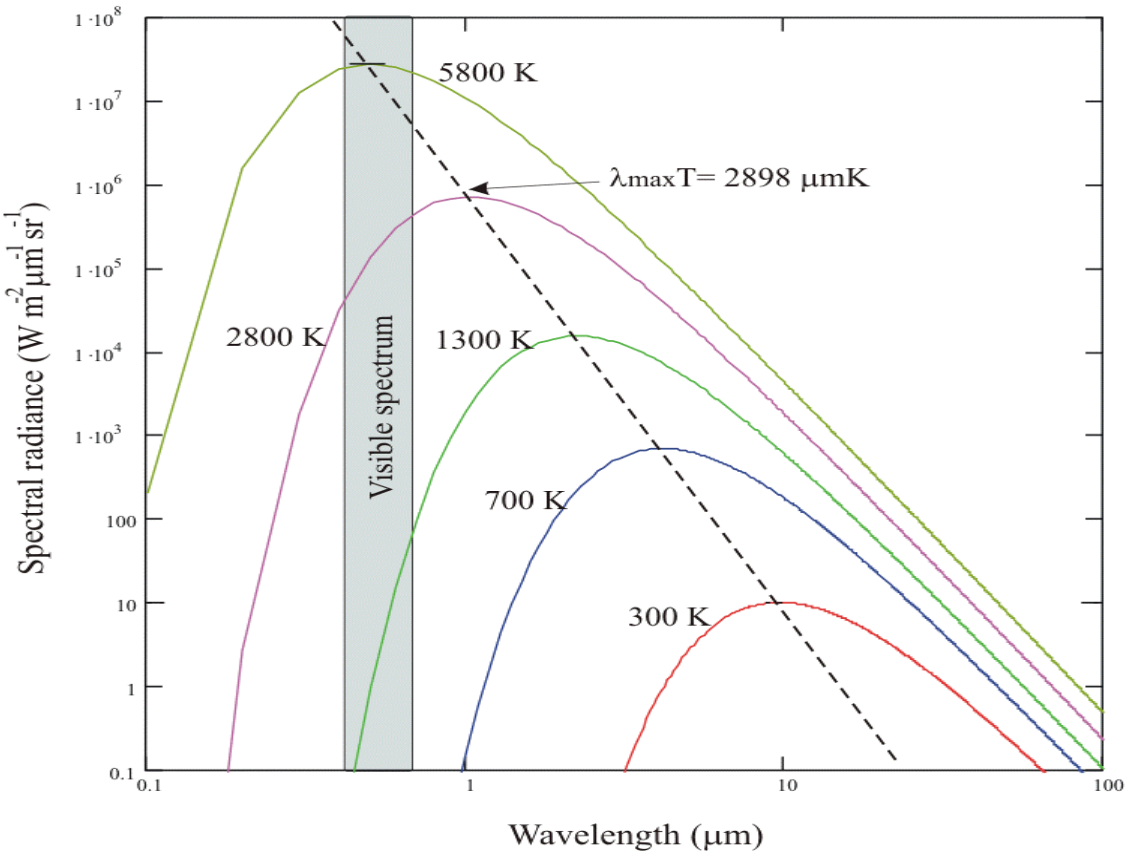

Fig. 1.1 Planck's law: the spectral radiance of a blackbody as a function of temperature.

Temperature (°C)	Color
500	Red, just visible
700	Dull Red
900	Cerise
1000	Bright cerise
1100	Dull orange red
1250	Bright orange yellow
1500	White
1800	Dazzling white

Table 1.1 Temperature versus perceived color.

Spectral radiance, measured versus the energy emitted per unit time by a surface per unit area, per unit wavelength, per unit solid angle is the technical term for the optical brightness of a surface. The advantage of using radiance, rather than other optical quantities, is that radiance is independent of distance to the surface and the size of the surface. Also for an ideal optical system of lenses and mirrors, the radiance of an object is constant. That means that the radiance is a constant in any optical system. Instruments that measure radiance allow us to infer temperatures at a distance and, if necessary, to use close-up or telephoto lenses.

A *blackbody* is simply a perfectly black surface: a perfect emitter and absorber of radiation [3]. Those who first encounter the blackbody concept may find it paradoxical, our every day experience is that bright objects are white because they reflect, not because they emit. For any object the ability to absorb (absorptivity) is the same as its ability to emit (emissivity). If not we could find situations where heat would flow from cooler temperatures to hotter temperatures, in contradiction to the basic laws of thermodynamics.

Objects have three basic optical properties: *emissivity*, *reflectivity and transmissivity*. Since any light falling on a surface must be either absorbed, reflected or transmitted,

$$Reflectivity + Emissivity + Transmissivity = 1 \qquad (1.1)$$

Or using the appropriate symbols,

$$\rho + \varepsilon + \tau = 1 \tag{1.2}$$

Most of the objects encountered in radiation thermometry are opaque so transmissivity is zero. In that case the reflectivity and emissivity are complementary properties. Fig. 1.2 gives a simple pictorial explanation of the relationship between reflectivity and emissivity for two different opaque surfaces.

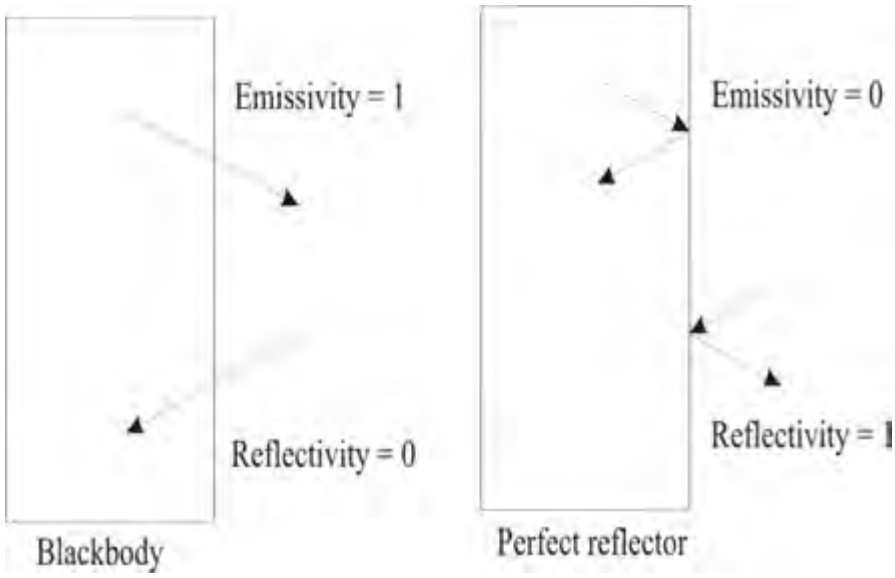

Fig.1.2 The complementary properties of emissivity and reflectivity

In 1900, Planck derived the mathematical description of the distribution of spectral blackbody radiation and is graphically shown in Fig. 1.1

$$L_{\lambda b}(\lambda, T) = \frac{c_1}{\lambda^5}\left[\exp\left(\frac{c_2}{\lambda T}\right) - 1\right]^{-1} \tag{1.3}$$

Where L_λ is the spectral radiance, the subscript *b* indicates that the radiance is that of a blackbody, λ is the wavelength of the radiation and *T* is the temperature of the blackbody in Kelvins.

The two constants c_1 and c_2 are known as the first and second radiation constants, and their best measured values are currently

$c_1 = 1.191044x10^{-16}$ [Wm^2]

and

$c_2 = 0.014388$ [m K]

In practice, real objects are not blackbody, but emit less radiation than predicted by Planck's law by the factor ε, the emissivity of the surface. The spectral radiance of a real object is

$$L_\lambda(\lambda,T) = \varepsilon(\lambda)L_{\lambda b}(\lambda,T) \qquad (1.4)$$

where $\varepsilon(\lambda)$ indicates that the emissivity may vary with wavelength.

All of the curves in Fig 1.1 are characterized by a maximum that occurs at shorter wavelengths as the temperature increases. The wavelength at which the maximum occurs is

$\lambda_{max} = 2989 / T$ [μm] (1.5)

At room temperature (*T = 300 K*), for example, the maximum spectral radiance is near *10* μm, and at *3000* K, the temperature of incandescent lamp filament, the peak occurs at *1* μm. For the objects of practical interest most of the radiation is emitted in the infrared portion of the spectrum. It is interesting to note that the response of the human eye has evolved to match the peak in the solar spectrum near *500* nm (*T = 5800 K*).

For several practical reasons, most radiation thermometry is carried out at wavelengths in the *0.5* μm to *20* μm portion of the spectrum, depending mostly on the temperature of interest. In the normal operating regime, λ is less than λ_{max}, and Planck's law is approximated to *1%* or better by *Wien's law*:

$$L_{\lambda b}(\lambda, T) = \frac{c_1}{\lambda^5}\left[\exp\left(\frac{-c_2}{\lambda T}\right)\right] \tag{1.6}$$

Although it is less exact because of the minor simplification, this is much more 'user-friendly' function than Planck's law for estimating the errors and uncertainties in measurements.

The total radiance of a blackbody, $L_b(T)$, is found by integrating Planck's law to determine the area under the curves of Fig. 1.1:

$$L_b(T) = \frac{\sigma}{\pi}T^4 \tag{1.7}$$

Where σ is the Stefan-Boltzman constant, $\sigma = 5.67051 \times 10^{-8}$ $Wm^{-2}K^{-4}$. The total power emitted by the blackbody in all directions is π times this value; hence energy is emitted by a real surface at the rate of

$$M = \varepsilon\sigma T^4 \qquad (1.8)$$

Where ε is the total emissivity. Some examples of the power emitted by blackbodies are given in table 1.2. Both the table and the fourth-power law in equation (1.8) show that the total radiance increases very rapidly with the temperature. At the short-wavelength end of the Planck spectrum the spectral radiance increases spectacularly.

Temperature (°C)	**Rate of emission (per square meter)**
25 (room temperature)	470 W
230 (melting point of solder)	3.6 kW
500 (a hot stove element)	20 kW
1000 (yellow flame)	150 kW
2500 (lamp filament)	3.4MW
5800 (sun)	77 MW

Table 1.2 The rate of emission of blackbodies at range of temperatures.

1.3 Errors in Spectral Band Thermometry

Every measurement made with a radiation thermometer involves the characterization of the sensor and transmission path, which change with each new measurement and are often inaccessible parts of the thermometer [2].

That part of the thermometer that we normally describe as the radiation thermometer is, strictly speaking, only a radiometer. The radiometer, which measures

radiance, is analogous to the potentiometer or voltmeter in a thermocouple circuit; only when the potentiometer is attached to the thermocouple do the two, together form a thermometer.

The errors in radiation thermometry fall into three main groups:

1. Errors relating to the characterization of the target surface (sensor): emissivity, reflections and fluorescence;
2. Errors due to variation in the transmission path: absorption and emission, scattering, size-of-source effects and vignetting; and
3. Signal processing errors due to variations in ambient temperature, linearization and the instrumental emissivity.

The radiometric measurement of the temperature of a real object requires knowledge of two, sometimes three quantities: the surface emissivity, the spectral radiance of the surface and, if a low-temperature thermometer is being used, the detector temperature. Many of the dominant errors that occur in spectral band thermometry can be interpreted as errors in either the measured radiance or the estimated emissivity.

The temperature error caused by errors in the measured radiance and emissivity is estimated as

$$\Delta T_m = \frac{\lambda T^2}{c_2}\left(\frac{\Delta L_m}{L_m} - \frac{\Delta\varepsilon(\lambda)}{\varepsilon(\lambda)}\right) \qquad (1.9)$$

Here ΔL_m represents the difference between the measured and true values of spectral radiance, and $\Delta\varepsilon(\lambda)$ represents the difference between the value of the instrumental emissivity and the true value of the emissivity, ε_i-$\varepsilon(\lambda)$.

Equation (1.9) is appropriate when the errors are known, but if the errors are unknown, then their relationship to the measurement error is properly expressed in terms of uncertainty:

$$\sigma_{Tm} = \frac{\lambda T^2}{c_2}\left(\frac{\sigma_{Lm}^2}{L_m^2} + \frac{\sigma_{\varepsilon(\lambda)}^2}{\varepsilon^2(\lambda)}\right)^{1/2} \tag{1.10}$$

This equation is conveniently expressed as

$$\sigma_{Tm} = \lambda\left(\frac{T}{1200}\right)^2\left(\rho_{Lm}^2 + \rho_{\varepsilon(\lambda)}^2\right)^{1/2} \tag{1.11}$$

where λ is in micrometers and the relative uncertainties, ρ, are in percent. For all three of these equations we can make the following observations:

- The errors and uncertainties increase with operating wavelength; therefore, as a general rule, choose thermometers with a short operating wavelength.
- The errors and uncertainties increase as the square of temperature.
- The errors and uncertainties due to emissivity as $1/\varepsilon(\lambda)$. In general, the errors are very large for low-emissivity materials, such as metals.

The wavelength dependence of errors can cause confusion when thermometers of differing operating wavelengths are used to measure the same temperature. Indeed, a difference in readings between two thermometers would normally indicate that both are probably in error, since nearly all the mayor sources of error are wavelength dependent and affect all spectral band thermometers.

1.3.1 Errors in emissivity

In almost all areas of radiation thermometry the largest source of error is the lack of knowledge about the surface emissivity. Depending on the degree of oxidation, roughness and wavelength, the emissivity varies, for example, between *0.1* and *0.95* in various samples of Inconel®. And this is a material that is used as emissivity standard.

For many materials, especially rough and amorphous materials, the practical problems are not as bad as implied. It is reasonably easy to identify the material, decide whether it is rough or polished, oxidized or not and make and estimate of the emissivity. However, to make a good estimate of the emissivity some serious homework is necessary. It is important to know what wavelength the thermometer operates at, and what the material is, and to have access to reliable information on the surface properties of the material. Most manufacturers of radiation thermometers supply a list of the emissivities of a wide variety of materials, each measured at the operating wavelength of their thermometer. If all of this information is available, it is usually possible to make an estimate to about *±0.05*.

At moderately high temperatures, where short-wavelength thermometers operate and the emissivity of materials is usually high, measurements can be made with reasonable accuracy. At lower temperatures, where the longer-wavelengths thermometers must be used and some materials have very low emissivities, the uncertainties can be so large as to make the measurements almost useless.

Without information on the spectral emissivity of the material, it is almost impossible to make reasonable estimate of the emissivity from the visual assessment alone. Surfaces that are black in the visible portion of the spectrum may well have a low emissivity in the infrared and vice versa. Two common examples will illustrate this point. Nowadays, most paints use titanium dioxide as the base pigment. While the pigment is extremely white (i.e. has a low emissivity) in the visible part of the spectrum, it is also very black in the infrared. Thus the appropriate emissivity setting for a *10* μm thermometer looking at any painted surface is about *0.95*. As a general rule most organic materials, for example wood, skin and organic fibers, exhibit this type of behaviour.

The opposite effect occurs with metals coated with thin layer of oxide. At short and visible wavelengths the surface can be quite black. At longer wavelengths the oxide layer becomes transparent so that the surface behaves as the pure metal and has a very low emissivity. For most surfaces the emissivity is also dependent on the angle of view. This is shown in Fig. 1.3. The drop in emissivity at high angles, which is for view near grazing incidence, is a feature in common with all surfaces. As a general rule the emissivities that

are published are for normal incidence, so radiation thermometers should always be used at or near normal incidence.

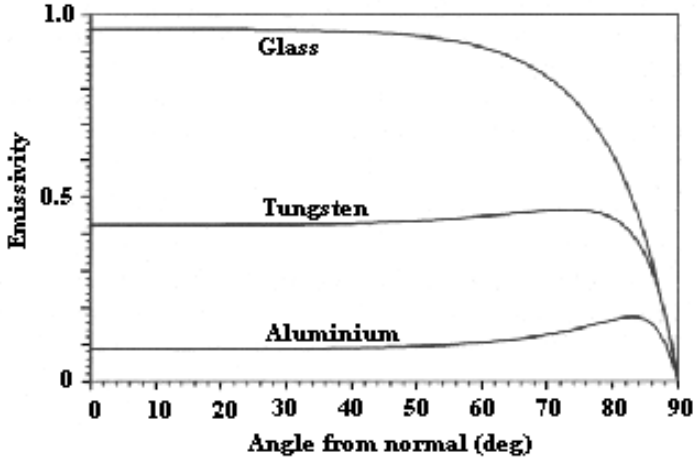

Fig. 1.3 The emissivity of glass, aluminum, and tungsten as a function of the angle of view [1].

1.3.2 Reflection errors

Because radiation thermometers infer temperature from measured radiance, anything that adds to the surface radiance will cause the thermometer to be in error. The most important source of additional radiance is radiation reflected from other objects in the vicinity. Radiation thermometers are most useful in for high temperature processing industries where, unfortunately, there are invariably reflections from flames, electric heaters, furnace walls, etc. At low temperatures the problem is even worse because the whole environment behaves as a very large blackbody at *300* K. In fact it is quite hard to find an application where reflections are not a problem.

The most difficult aspect of the reflection problem is that we do not naturally associate other hot objects, which may be some distance from the source of interest, with the surface itself. It is a matter of discipline to be aware of all objects in the space above a surface and methodically assess the likelihood of reflection error caused by that object.

The most effective way of eliminating reflection errors is to eliminate the source of extraneous radiation. One of the most important sources of radiation in measurements made outdoors is the sun. If a radiation thermometer is being used to detect hot spots, such as thermal leak in buildings, then the measurements should be made when the surface is shaded, or at night. In many cases it is possible to shade the surface artificially. This technique can also be used inside furnaces to shade heaters or flames that are in close proximity to a surface.

More often than not, the interfering source is too large or too hot to shade. This occurs in many high temperature processing industries where a product is pre-heated in a large firebox, and radiation thermometers are used to determine when the product has reached the required temperature. Fortunately, in these cases it is relatively easy to estimate the magnitude of errors. If we assume that the firebox walls are at a uniform temperature, T_w, Then the firebox behaves as a blackbody cavity with an emissivity of 1.0. The radiance of a small object within the firebox then comprises two parts:

$$L_m = \varepsilon(\lambda)L_b(\lambda,T_s) + [1-\varepsilon(\lambda)]L_b(\lambda,T_w) \qquad (1.12)$$

The first part of the equation represents the thermal emission from the surface, and the second is the radiance due to reflections originating from the firebox walls. Now, depending on the wall temperature, T_w there are four strategies for handling the reflection.

1. $T_W << T_S$: assume negligible error and set $\varepsilon_i=\varepsilon(\lambda)$.
2. $T_W \cong T_S$: assume black body conditions and set $\varepsilon_i=1.0$
3. $T_W >> T_S$: apply corrections for reflections (high temperatures). For these systems there is an optimum operating wavelength that minimizes the uncertainty in the corrected result. $\lambda_{opt,}$ is near

   $$\lambda_{opt} \approx c_2 \frac{(T_w - T_s)}{T_w T_s}$$

4. $T_W \cong T_S$ apply corrections for reflections (low temperatures). Almost all low-temperature measurements are therefore corrupted by the reflected radiation from the walls. If we correct for the emissivity and then for the detector radiance we obtain

   $$L_m = L_b(\lambda, T_s) + \frac{[1-\varepsilon(\lambda)][L_b(\lambda, T_w) - L_b(\lambda, T_d)]}{\varepsilon(\lambda)}$$

   Thus the reflection error is zero if the detector and the surroundings are at the same temperature. This requirement is very nearly satisfied for measurement made indoors since our rooms behave very much like a black body as the same temperature as the thermometer.

1.3.3 Absorption errors

One of the great advantages of radiation thermometers is that they can measure temperature at a distance. However this involves using the intervening space between the object and the thermometer as the transmission path for the radiation, and unfortunately most gases, including air, are not completely transparent. Most of the absorption in air (Fig. 1.4) is due to water vapor and carbon dioxide.

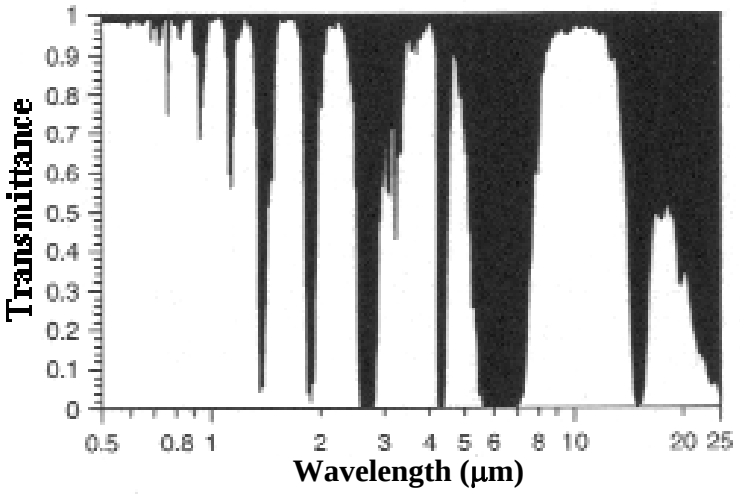

Fig.1.4 The transmittance of *300*m of air at sea level. The area above the transmittance of the spectrum for which the atmosphere is transparent (unshaded) are known as windows. Some of the most useful windows for spectral band radiation thermometry are near *0.65* μm, *0.9* μm, *1.05* μm, *1.35* μm, *1.6* μm, *2.2* μm, *4* μm and *10* μm [1].

Nearly all spectral band thermometers are designed to avoid the worst of the absorption bands, and in most practical situations the absorption effects can be neglected. However, most of the thermometers operate over a broad band of wavelengths that overlaps the tails of the absorption lines and will not be completely immune to these effects. When

they are used in environments with very high concentrations of carbon dioxide and water, such as inside oil-or gas-fired furnaces, they are sensitive to absorption effects. Where the gas is hotter than the target the thermometer will read high and vice versa. The worst cases are in the exhausts of flames where there are high concentrations of water and carbon dioxide at high temperatures. Errors approaching *10* °C per meter of path length have been observed. Absorption errors are also a problem for some general-purpose low temperature thermometers because they employ very wide bandwidths, such as from *8* μm to *20* μm, which includes water absorption lines.

When absorption errors occur they can be modeled by an equation of the same form as that for the reflection errors:

$$L_{m,a} = \alpha(\lambda)L_b(\lambda,T_g)d + \left[1 - \alpha(\lambda)d\right]L_m \qquad (1.13)$$

where $\alpha(\lambda)$ is the absorption coefficient of the gas, d is the path length through the gas, T_g is the gas temperature, and L_m is the radiance of the surface that would be measured in the absence of the gas. The effect of the gas absorption is almost identical to reflection errors (except that it varies with path length, d), so there are three similar measurement strategies:

1. $T_g << Ts$: the absorption in the gas appears to reduce the emissivity of the target.
2. $T_g \cong T_s$: the gas and the target behave much like a blackbody.
3. $T_g >> T_s$: the emission from the gas appears to increase the emissivity of the target.

In principle, we could use Equation (1.13) to calculate corrections for the absorption. In practice, however, there are large uncertainties associated with the values of the absorption coefficient and gas temperature. In addition, the effect often occurs in combination with reflection errors, with the result that the uncertainties in the corrections are impractically large.

A key factor in Equation (1.13) is that the absorption effect increases with the distance. Thus the error can be detected, and the magnitude of the error estimated, by observing the same target through different distances, thereby changing the path length through the interfering gas.

1.3.4 Transmission errors

With transparent objects, radiation from behind the target can find its way to the radiometer. This situation arises most commonly with glass and plastics. Models of the situation are almost identical to those for reflection and absorption, and as expected the strategies for avoiding the errors are similar. If the object behind is sufficiently cool, there is no error. If the object behind is at similar temperature, it enhances the effective emissivity of the object to a value near 1.0. If the object behind is hotter it can cause large errors. The error can be detected by changing the temperature of the background, perhaps by placing a different object behind the object of interest. For situations in glass and plastics there are radiation thermometers specially designed to avoid these errors.

1.3.5 Non-thermal emission

Another, less frequent, source of error is fluorescence, which arises because thermal energy excites impurities in the object that then emit radiation in a very narrow band of wavelength. This can happen with some type of glass.

If this type of non-blackbody emission occurs with the pass-band of the radiation thermometer, then the measured radiance will be high. The problem is most likely to occur in relatively pure materials that are partially transparent in the pass band of the thermometer.

Avoiding errors due to fluorescence is difficult unless equipment is available to measure the whole spectrum. The best strategy is to use well-established procedures and operating wavelengths. This relies on the fact that others have found such procedures reliable.

1.3.6 Scattering errors

Dust in the transmission path of the radiation thermometer has three detrimental effects. First, it scatters radiation out of the transmission path. This cause a decrease in the measured radiance of the object of interest, and therefore a decrease in the temperature readings. Second, it scatters radiation from other sources into the transmission path and

increases the temperature reading. Third, the dust may itself emit blackbody radiation, so that the dust temperature will affect the thermometer reading. Examples of dust include smoke, luminous flames, water fog, carbon, metal ore, and silica. The *2 %* to *3 %* loss in transmission in the windows in Fig. 1.4 is due to atmospheric scattering.

The general problem of the scattering of radiation from small particles is extremely complicated and depends on the size of the particles, on whether they transmit or absorb, and on the wavelength of the radiation. The only useful general principle is that the problem can often, but not always, be reduced by using thermometers that operate at longer wavelengths.

1.3.7 Size of the source effects

All radiation thermometers collect the radiation from a well-defined conical zone in front of the thermometer (Fig. 1.5). The size of the zone is defined by the two defining apertures and is known as the field of view. Ideally, the zone has a sharp boundary so that radiation from outside the cone has no effect on the reading. In practice, there are three effects, as shown in Fig. 1.5, which contribute to the blurring of the field of view boundary.

Flare

It is the most serious of the size-of-source effects. It is caused by scattering of radiation within the radiation thermometer; in particular, by dust, scratches and density imperfections on, or in, the front lens of the thermometer. Usually the only way to

minimize flare is to use sight tubes. These are tubes which are black on the inside, and mounted on the front of the thermometer to restrict the radiation falling on the lens to that within the field of view. When employing sight tubes it is important that the tube does not impinge on the field of view, as this will cause vignetting.

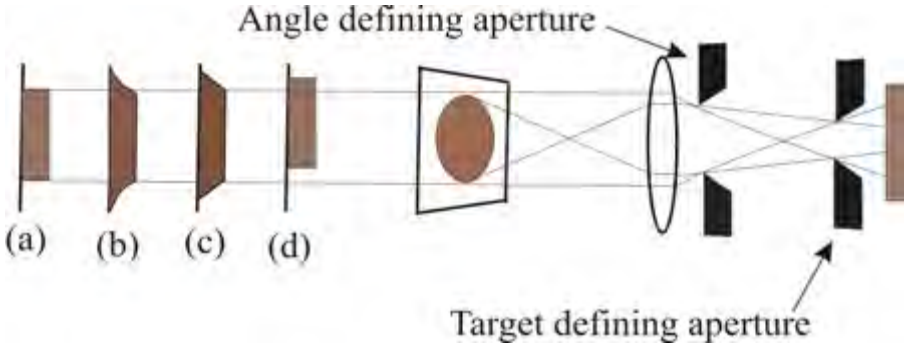

Fig 1.5 Size-of-source effects: (a) an ideal target profile, (b) a target profile broadened by flare, (c) a target profile due to poor focus, and (d) misalignment.

Poor focus

Lenses and mirrors in radiation thermometers are used to focus an image of the object of interest onto the target-defining aperture. Radiation from the portion of the image over the aperture then passes on to detector. If the thermometer is not well focused then the boundaries of the target area are not well defined, Fig1.5 (c). For systems with a fixed focus or no lenses, the field of view must be well overfilled in order to get an accurate reading.

Optical aberrations and misalignment

In practice, imperfections in the optical components, interelement reflections, and slight misalignment of the optical components all lead to very slight blurring of the target image. Usually these effects are negligible for practical purposes. However there are two examples of misalignment that lead to large size-of-source problems. The first occur if, the thermometer is knocked or dropped, so that some of the components become seriously misaligned. The second problem occurs in long-wavelength thermometers where a separate visual telescope or sighting laser is provided to sight the target. If the two optical paths are not exactly aligned, or not in focus at the same time, then the field of view may have to be overfilled considerably to get an accurate reading. To minimize effects, always overfill the field of view as much as possible with neighboring objects at the same or similar temperature as the object of interest. In particular, avoid having objects at a much higher temperature than the object of interest near the field of view.

Ambient temperature dependence

All radiation thermometers suffer some sensitivity to the ambient temperature due to any one of three causes. A cause that affects all radiation thermometers is the change in detector sensitivity with temperature. In most radiation thermometers, there is an electronic means of compensating the change in sensitivity. However, if the ambient temperature changes quickly the compensation is unlikely to track the change in detector temperature exactly. For this reason thermometer should be allowed to settle in a new environment for up to an hour to ensure that the whole instrument has come to equilibrium.

In instruments with very narrow bandwidths, the wavelength response is determined by the pass-band of interference filters, which are extremely sensitive to temperature. Low-temperature and long-wavelength radiation thermometers are probably the most susceptible to ambient temperature changes. This is because the signal from a detector in radiation thermometer is actually a measure of the difference between the radiance of the target and the radiance of the detector. For high-temperature applications, the detector radiance is negligible and is ignored. However, for thermometers working below *200* °C, and especially those working near 20 °C or lower, the detector radiance is significant and may be greater than that of the object of interest. For these instruments it is necessary to measure or compensate for the detector radiance in order to achieve an accurate measurement.

Vignetting

In all radiation thermometers the acceptance angle and the target area are defined by the two apertures (Fig.1.5). Anything that further restricts the cone of radiation accepted by the thermometer will cause the thermometer to read low, since there will be less radiation falling on the detector. In particular, all parts of the front lens of the thermometer must have an unobstructed view of the entire target. Obstruction of the field of view, known as vignetting, occurs often in high temperature applications where the thermometer is sighted through small peepholes in furnace walls. Vignetting also occurs when sight tubes are misaligned.

Linearization

All direct-reading radiation thermometers include some form of linearization in their electronic systems. This is necessary to convert the signal from the detector, which is an extremely non-linear function of temperature, into a signal that is proportional to temperature.

1.4 The dual wavelength thermometer

In some applications the uncertainty in emissivity seriously limits the utility of spectral band thermometers, an useful alternative are the ratio thermometers. Dual-wavelength thermometers also known as ratio thermometers and two-color thermometers, measure radiance at two wavelengths and determine the ratio

$$R = \frac{\alpha(\lambda_1)\varepsilon(\lambda_1)L_b(\lambda_1, T_s)}{\alpha(\lambda_2)\varepsilon(\lambda_2)L_b(\lambda_2, T_s)} \tag{1.14}$$

If it is assumed that the absorption $\alpha(\lambda)$ and the emissivity $\varepsilon(\lambda)$ are constant over the wavelength range including λ_1 and λ_2, then the ratio R depends only on the temperature.

The independence from emissivity and absorption is obtained at the expense of sensitivity. This can be seen firstly from Wien's law approximation for R,

$$R = \left(\frac{\lambda_2}{\lambda_1}\right) exp\left[\frac{c_2}{T}\left(\frac{1}{\lambda_2} - \frac{1}{\lambda_1}\right)\right] \tag{1.15}$$

And secondly from the propagation-of-uncertainty formula which gives the uncertainty in temperature versus the uncertainty in R:

$$\varsigma\sigma_{Tm} = \frac{\lambda_1\lambda_2}{\lambda_1 - \lambda_2}\frac{T^2}{c_2}\frac{\sigma_R}{R} \tag{1.16}$$

The similarity of these equations to those for the single-wavelength spectral band thermometers suggests that the performance of the ratio thermometer would be similar to that of a spectral band thermometer with an operating wavelength of

$$\lambda_e = \frac{\lambda_1\lambda_2}{\lambda_1 - \lambda_2} \tag{1.17}$$

However, this is misleading. While the sensitivity is 10 to 20 times worse than a good spectral band thermometer, some of the most significant errors are also much less important. First, the most significant error in spectral band thermometry, the uncertainty in emissivity, has been eliminated. And second, many of the instrumental errors that affect the radiance measurement in spectral band thermometers are common to both channels of the ratio thermometer and so do not affect the ratio.

Overall the performance of ratio thermometers on surfaces that have a high emissivity and are grey (i.e. constant emissivity with wavelength) is perhaps two or three times worse than good spectral band measurements. On the other hand, if the surface is grey and has a low or highly variable emissivity (with time or temperature) then the ratio thermometer is clearly better. Ratio thermometers find application where the object is too small to fill the field of view and a spectral band thermometer would be susceptible to size-of-source effects. Such objects include hot wires and molten-glass streams.

References

[1] J.V. Nicholas, D.R. White, Traceable Temperatures, An introduction to Temperature Measurement and Calibration. 2nd Ed. Wiley, chapter 9, (2004).

[2] D.P. DeWitt and G.D. Nutter, Theory and practice of Radiation Thermometry, Wiley Interscience, New York (1988).

[3] T.J. Quinn, Temperature, 2nd Edition, Academic Press, London (1990).

Chapter 2

Detected incidance from a thermal source in a wavelength interval

2.1 Introduction

To assess the total amount of radiation emitted in a wavelength interval, requires the integration of the Planck's equation. In this chapter we use an alternative method of integrating the Planck's equation. The amount of signal that a detector register, depends on its general type, its sensitivity and its non-radiometric characteristics. The incidance from a grey body source detected in the wavelength interval is determined for a quantum and thermal detectors, for the ideal behavior. We applied these results to the specific case of a tungsten thermal source, an important calibration source for spectrometric applications.

2.2 Responsivity of the thermal and quantum detectors

Before we evaluate the amount of radiation detected by a detector at a given temperature, we review some parameters that are useful in modeling its behavior. These parameters or figures-of-merit are relevant because they allow us to deduce the detection limits[1,2]. Generally, we are interested in the sensor performance with respect to the power incident upon the sensor and the minimum detectable power. Sometimes we use the term *sensitivity* to describe the ratio of change in its input. This word is ambiguous because

it is used in so many different ways. Hence, we will use the following terms: *responsivity, noise equivalent power, signal-to-noise ratio, and detectivity*.

First, we need to know the root mean square (*rms*) signal voltage $V_{S(rms)}$ (or current $I_{S(rms)}$) generated in a detector with a temperature T_D in response to an average incident radiant power *P*. Although the detectors may be modeled as either sources of current or voltage, we will treat them as generating voltage quantities. This is possible because the ease of transformation between a current to voltage source. Generally the measured current, voltage, even the radiant power exhibit some fluctuation. We are interested in a *rms* values throughout this study, unless we say otherwise, the current and voltage quantities are *rms*ed. The noise *rms* is measured with the detector covered (so the incident radiant power is zero). Considering that the signal and the noise voltages are temperature dependent, the signal to noise ratio is evaluated at temperature T_D then it is defined as

$$SNR(T_D) = V_S(T_D) / V_n(T_D) \qquad (2.1)$$

The spectral responsivity $R(T_D,\lambda)$ is defined as the ratio of the (output) signal voltage to the radiant power *P* incident upon the detector.

$$R(T_D,\lambda) = V_S(T_D)/P(\lambda) \qquad \text{[V/W]} \qquad (2.2)$$

The units utilized will depend on the type of detector and its intended use; however, normally these will be volts (or amps) per watt. We see that the responsivity changes with wavelength.

It is difficult to measure the signal voltage when it is equal to that generated by the noise. The noise equivalent power *NEP* is the incident radiant power that produces an output voltage equal to that noise. We would interpret the *NEP* as an indication of the minimum detectable signal. We can calculate the spectral *NEP* as

$$NEP(T_D, \lambda) = \frac{P(\lambda)}{SNR(T_D)} \qquad \text{[W]} \qquad (2.3)$$

The *SNR* depends on several characteristics of the detector, including the temperature T_D, its area A_D, and the bandwidth Δf. Therefore, the *NEP* also depends on these characteristics. Many noise sources generate white noise, for which the square of the noise voltage is proportional to the electrical bandwidth Δf. In addition, for a large number of sensors, the noise voltage squared is proportional to the detector area A_D. Thus the noise voltage (or noise current) is proportional to squared root of the product of bandwidth and area. Hence we may define the normalized *NEP** as follows:

$$NEP^*(T_D, \lambda) = \frac{NEP(T_D, \lambda)}{\sqrt{A_D \Delta f}} \qquad \text{[W/ (cm Hz)}^{1/2}\text{]} \qquad (2.4)$$

Thus, the *NEP** is independent of the detector size and electrical bandwidth. However, a large *NEP** refers to a poor detector performance. For this reason, the reciprocal of the *NEP** is commonly used because it incorporates a direct relationship with a superior performance of the detector. This quantity is called the specific detectivity *D** (pronounced D-star) and defined as

$$D^*(T_D,\lambda)=\frac{\sqrt{A_D\Delta f}}{NEP(T_D,\lambda)} \qquad [\text{cm Hz}^{1/2}/\text{W}] \qquad (2.5)$$

Upon combining Eqs. (2.1) and (2.2) and substituting them in Eq. (2.3), we may write the *NEP* in terms of responsivity

$$NEP(T_D,\lambda)=\frac{V_n}{R(T_D,\lambda)} \qquad [\text{W}] \qquad (2.6)$$

Finally, using Eqs. (2.5) and (2.6), the responsivity can be expressed as follows

$$R(T_D,\lambda)=\frac{D^*(T_D,\lambda)V_n}{\sqrt{A_D\Delta f}} \qquad [\text{V/W}] \qquad (2.7)$$

The optical detectors may be classified essentially as either thermal or quantum devices [3,4,5,6]. The power of the incident radiation raises the temperature of the thermal detector, inducing a change of some temperature dependent parameter. The thermal detectors measure the energy absorbed per unit time, whereas quantum detectors measure the rate of absorption of quanta.

The responsivity of an ideal thermal detector is independent of the wavelength, and constant for a given detector temperature. Then, Eq. (2.7) may be written

$$R(T_D,\lambda)=\frac{D^*(T_D)V_n}{\sqrt{A_D\Delta f}} \qquad [\text{V/W}] \qquad (2.8)$$

Figure 2.1 shows the response of ideal thermal and quantum detectors. The responsivity of a thermal detector is proportional to the absorbed radiant power, but is independent of the wavelength. The responsivity of the quantum detector (for equal amounts of radiant power per unit wavelength interval) increases with the wavelength. This behavior is a consequence of the fact that the number of photons per second per watt is directly proportional to wavelength. This functional dependence on wavelength persists until the photon energy is equal to the bandgap, i.e., the photon does not have enough energy to impart to electron to cross the gap.

Therefore, the quantum detector does not operate beyond this maximum wavelength λ_{max} Fig. 2.2 shows the specific detectivity as a function of wavelength for some representative photodetectors.

Using Eq. (2.7), the detectivity of an ideal quantum detector is given by

$$D^*(T_D, \lambda) = \frac{D^*(T_D, \lambda_{\max})}{\lambda_{\max}} \lambda \qquad [\text{mHz}^{1/2}/\text{W}] \qquad (2.9)$$

Thus, the responsivity of an ideal quantum detector finally be expressed as

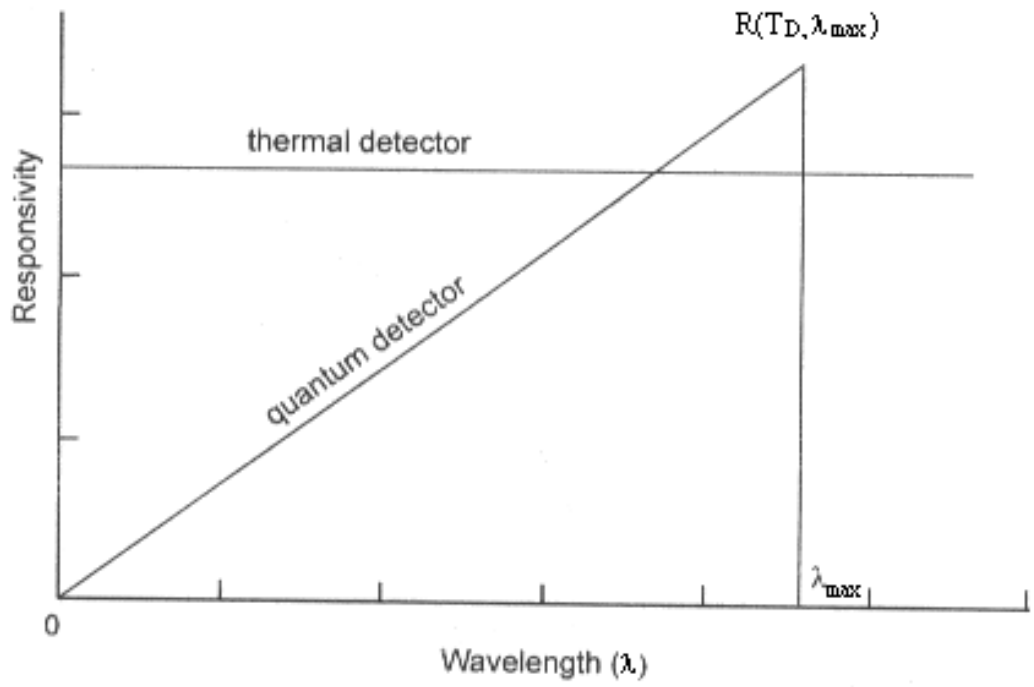

Fig. 2.1 Ideal behaviour of thermal and quantum detectors.

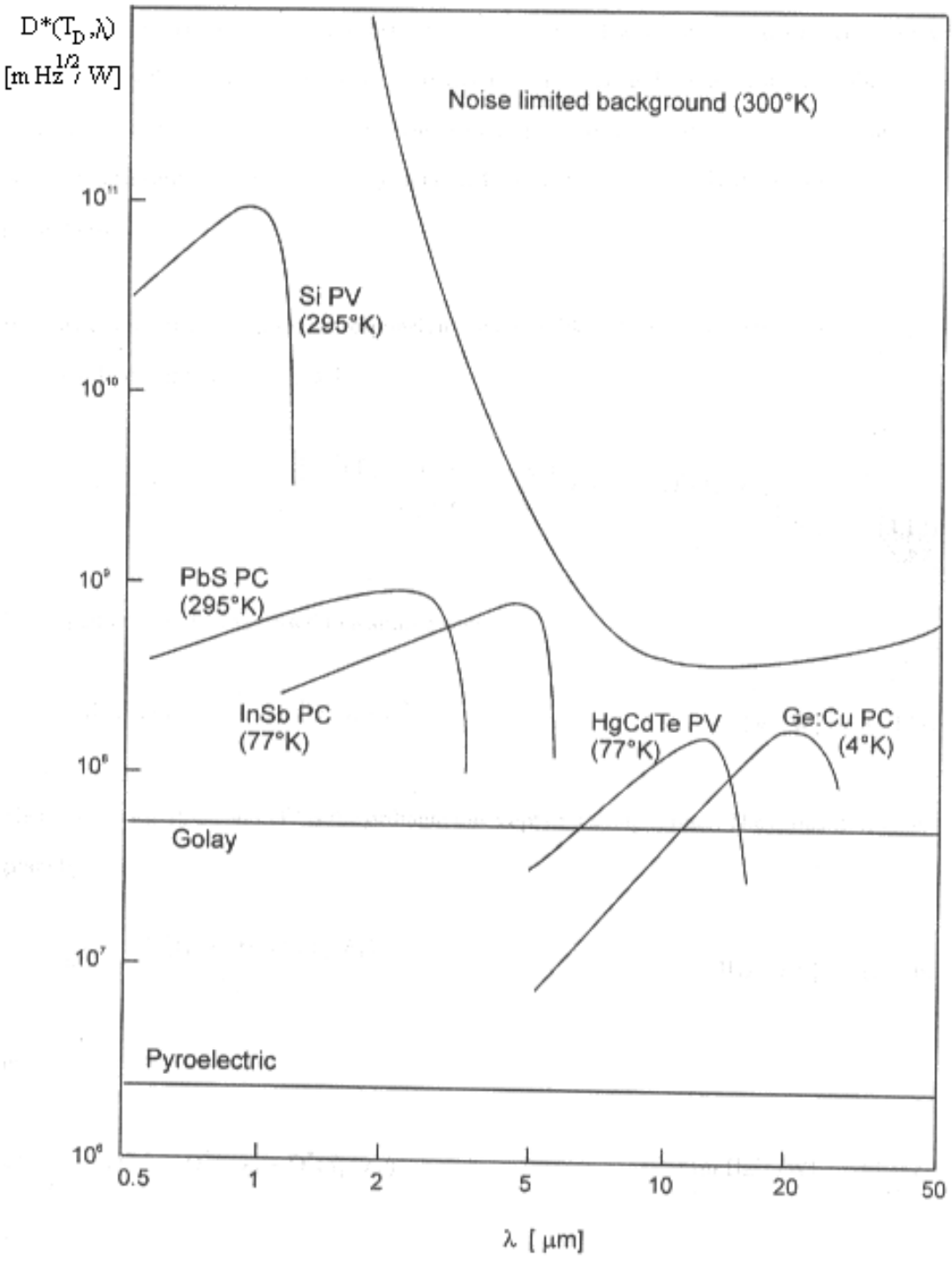

Fig. 2.2 Specific detectivity as a function of wavelength for some representative photodetectors. PV refers to photovoltaic device and PC to a photoconductive one.

$$R(T_D,\lambda)=\frac{V_n D^*(T_D,\lambda_{\max})}{\sqrt{A_D\Delta f}\,\lambda_{\max}}\lambda \qquad \text{[V/W]} \qquad (2.10)$$

We may rewrite the specific detectivity of an ideal quantum detector in order to simplify the notation. In many applications the detector temperature is kept constant, at T_D.

$$D^*(T_D,\lambda)=\frac{D^*(T_D,\lambda_2)}{\lambda_2}\lambda=\frac{D_2{}^*}{\lambda_2}\lambda \qquad \text{[mHz}^{1/2}\text{/W]} \qquad (2.11)$$

Here we assume that the maximum wavelength at which the detection is still possible is equal to the upper limit of the spectral interval of interest $[\lambda_1, \lambda_2]$. A detector is normally selected so that its spectral range of responsivity is larger or equal to this interval.

The responsivity of the quantum detector in the wavelength interval $[\lambda_1, \lambda_2]$, where λ_{max} is greater than λ_2, Eq. (2.11), is rewritten then as follows

$$R(T_D,\lambda)=\frac{V_n D^*(T_D,\lambda_2)}{\sqrt{A_D\Delta f}\,\lambda_2}\lambda=\frac{V_n D_2{}^*}{\sqrt{A_D\Delta f}\,\lambda_2}\lambda \qquad \text{[V/W]} \qquad (2.12)$$

The last equality is obtained upon substituting Eq. (2.11). The wavelength dependence of the absorption coefficient modifies the ideal behavior of the thermal detector. Likewise, the quantum efficiency η depends on altering the ideal response. Figure 2.3 shows both the ideal (unit quantum efficiency) and the typical current responsivity of a PIN photodiode. We may approximate the spectral responsivity of a non-ideal detector (quantum o thermal) as a straight line, depicted in Fig. 2.4.

$$R(T_D,\lambda)=\frac{V_n}{\sqrt{A_D\Delta f}}\left[\frac{D^*(T_D,\lambda_2)-D^*(T_D,\lambda_1)}{\lambda_2-\lambda_1}\right]\ (\lambda-\lambda_1)-D^*(T_D,\lambda_1)$$

[V/W] (2.13)

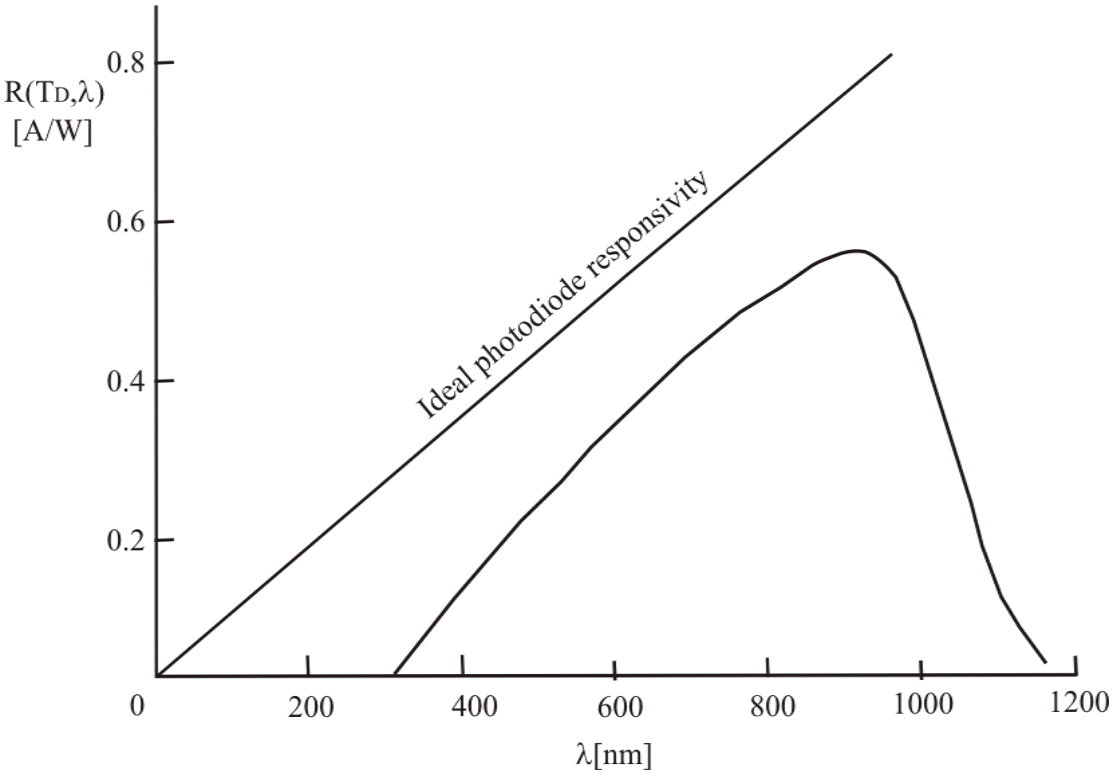

Fig. 2.3 Typical current responsivity of a PIN photodiode. The straight line represents the responsivity of an ideal photodiode with unit quantum efficiency.

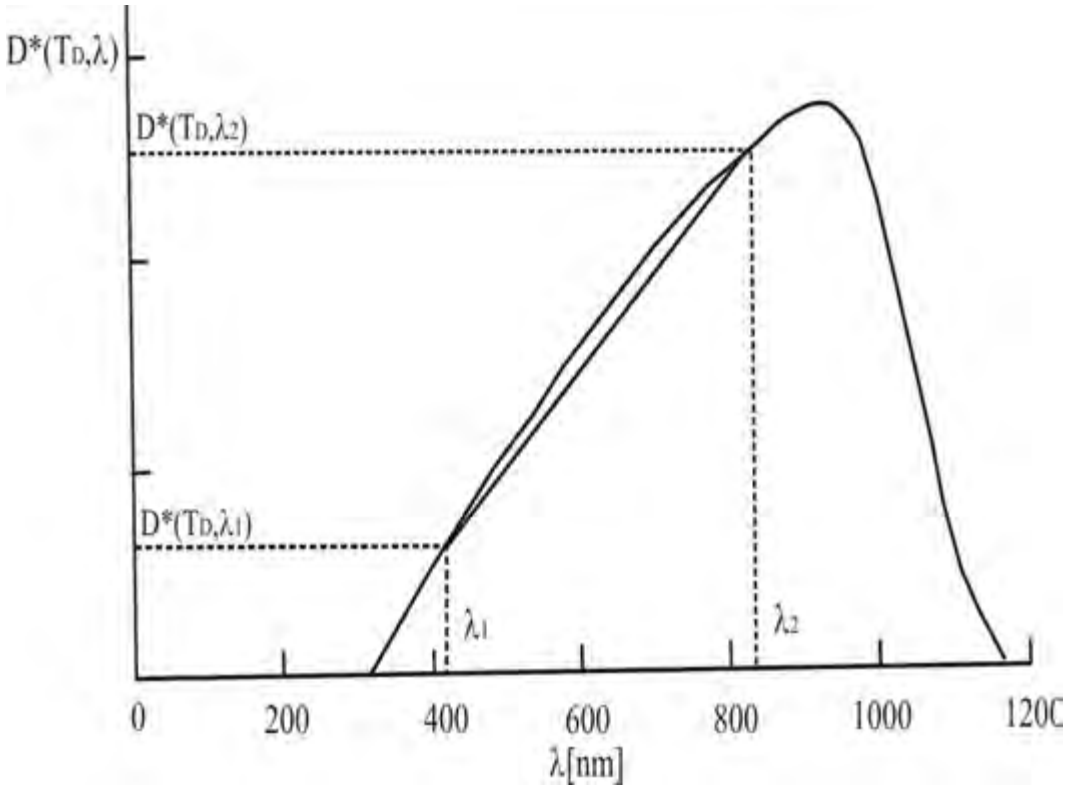

Fig. 2.4 The quantities used for the approximation of the spectral responsivity as a straight line in a wavelength interval.

2.3 Incidance from a thermal radiator in a wavelength interval

The spectral radiance $L_\lambda(T)$ is the spectral radiative power emitted per unit area per unit solid angle in the wavelength interval λ to $\lambda+d\lambda$. The spectral radiance of the radiation emitted from a black-body source at temperature T, also knows as the Planck's law, is

$$L_\lambda^{BB}(T) = \frac{1}{\lambda^5}\frac{2hc^2}{\left(\exp(\frac{ch}{\lambda kT})-1\right)} \qquad [\mathrm{W/(m^2.sr.\mu m)}] \qquad (2.14)$$

Where

^{BB} superscript refers to the blackbody radiation,

h is the Planck's constant (6.6256± 0.0005) x10^{-34} [J sec],

T is the absolute temperature in Kelvin degrees [K],

λ is the wavelength in [μm],

c is the velocity of the light in vacuum (2.992925±0.000003)x10^8 [m/sec], and

k is the Boltzmann's constant (1.38054±0.00018)x10^{-23} [JK^{-1}].

The spectral radiance of the black-body at various temperatures is depicted in Fig. 2.5. Eq. (2.14) is often written as follows

$$L_\lambda^{BB}(T) = \frac{c_1}{\pi\lambda^5}\frac{1}{\left(\exp(\frac{c_2}{\lambda T})-1\right)} \qquad [\mathrm{W/(m^2.sr.\mu m)}] \qquad (2.15)$$

Here, we do a small change of what we have in chapter 2,

c_1 is the first radiation constant = $2\pi hc^2$ = (3.7415±0.0003)x10^8 W.$\mu m^4 m^{-2}$

c_2.is the second radiation constant = c.h/k = (1.43879±0.00019)x10^4 µm.K.

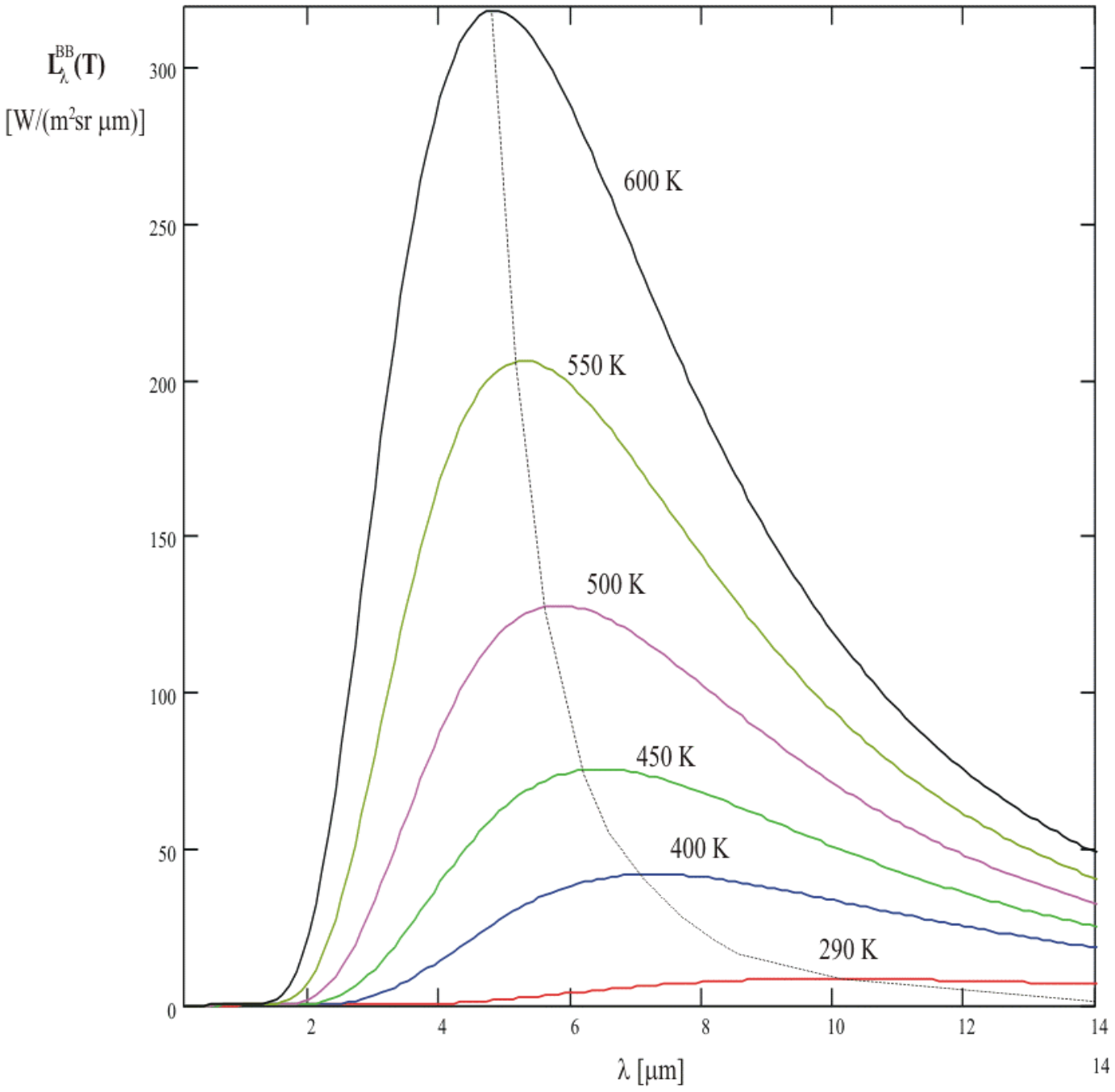

Fig. 2.5 Spectral radiance of a blackbody at different temperatures.

We are interested in the radiation incident per unit area at the detector $E_\lambda(T)$, assuming a Lambertian radiator. We start from an expression for the incidance onto the image plane of an optical system [8].

$$E_\lambda^{BB}(T) = \omega\tau L_\lambda^{BB}(T) \qquad [\mathrm{W/(m^2\mu m)}] \qquad (2.16)$$

Here $E_\lambda^{BB}(T)$ is the spectral incidance produced from a black- body source onto the image plane. In this equation τ is the transmission loss factor, a spectral quantity, in general. However when we design an instrument, its spectral interval of operation is customary chosen such that τ is constant. In addition, ω is the solid angle subtended by the optical system at the focal plane.

$$\omega = \pi(\sin^2\Theta_{\max} - \sin^2\Theta_{\min}) \qquad [\mathrm{sr}] \qquad (2.17)$$

Θ_{max} is the half angle that the optical system subtends at the detector and Θ_{min} is the half angle of the central obstruction. Substituting Eq. (2.15) in Eq. (2.16), we obtain

$$E_\lambda^{BB}(T) = \frac{c_1}{\pi\lambda^5}\frac{\omega\tau}{\left(\exp(\frac{c_2}{\lambda T}) - 1\right)} \qquad [\mathrm{W/(m^2\mu m)}] \qquad (2.18)$$

We can express the incidance of a natural, non-black body radiator, introducing the emissivity $\varepsilon(T,\lambda)$ that depends on temperature and wavelength.

$$E_\lambda(T) = \frac{c_1}{\pi\lambda^5}\frac{\omega\tau\varepsilon(T,\lambda)}{\left(\exp(\frac{c_2}{\lambda T})-1\right)} \qquad [\mathrm{W/(m^2\mu m)}] \qquad (2.19)$$

The spectral emissivity is thus a ratio of the radiation emitted from a natural radiator to that emitted by a black-body radiator. We want to evaluate the amount of radiation detected in the wavelength interval $[\lambda_1, \lambda_2]$ by a detector at temperature T_D with responsivity $R(T_D, \lambda)$. Therefore, we multiply the spectral incidance given in Eq. (2.19) by the responsivity $R(T_D, \lambda)$ to obtain the detected spectral incidance $E^D{}_\lambda(T)$.

$$E^D_\lambda(T) = \frac{c_1}{\pi\lambda^5}\frac{\omega\tau\varepsilon(T,\lambda)R(T_D,\lambda)}{\left(\exp(\frac{c_2}{\lambda T})-1\right)} \qquad [\mathrm{V/(m^2\mu m)}] \qquad (2.20)$$

To find the total detector output, we integrate the product of spectral incidance with the detector responsivity over the wavelength interval. This quantity is called the detected incidance, $E^D{}_{[\lambda 1,\, \lambda 2]}(T)$.

$$E^D_{[\lambda 1,\lambda 2]}(T) = \int_{\lambda 1}^{\lambda 2} \varepsilon(T,\lambda)R(T_D,\lambda)E^{BB}_\lambda(T)d\lambda \qquad [\mathrm{V/m^2}] \qquad (2.21)$$

We may substitute the spectral incidance of the black-body source $E_\lambda{}^{BB}(T)$.

$$E^D_{[\lambda 1,\lambda 2]}(T) = c_1\omega\tau\int_{\lambda 1}^{\lambda 2}\frac{1}{\pi\lambda^5}\frac{\varepsilon(T,\lambda)R(T_D,\lambda)}{\left(\exp(\frac{c_2}{\lambda T})-1\right)}d\lambda \qquad [\mathrm{V/m^2}] \qquad (2.22)$$

In the last expression, we factored out the terms that are independent of the wavelength. We keep in mind that the spectral dependence of the responsivity of a thermal detector is constant, that is, independent of wavelength (see Eq. (2.8)), and a straight line with a positive slope for an ideal quantum detector (see Eq.(2.10)). The detector responsivity depends strongly also on its operating temperature T_D. This temperature is generally controlled, so it varies insignificantly with the temperature, allowing us to neglect its temperature dependence.

2.4 Incidance detected with quantum and thermal detectors

In the previous section we obtained an expression for the detected incidance $E^D_{[\lambda 1,\, \lambda 2]}(T)$, after we integrated the product of radiative incidance with the detector responsivity over the wavelength interval. Now we are interested in calculating the detected incidance for thermal and quantum detectors. This may be achieved by employing the corresponding spectral responsivity of the detector.

2.4.1 Ideal quantum detector

We saw that an ideal quantum detector has responsivity with linear wavelength dependence. We substitute Eq. (2.12) into Eq. (2.22) to obtain the incidance detected with a quantum detector.

$$E^D_{[\lambda 1,\lambda 2]}(T) = c_1 \omega \tau \int_{\lambda 1}^{\lambda 2} \frac{1}{\pi \lambda^5} \frac{\varepsilon(T,\lambda)}{\left(\exp(\frac{c_2}{\lambda T}) - 1\right)} \frac{V_n \lambda}{\sqrt{A_D \Delta f}} \frac{D_2^*(T_D, \lambda_2)}{\lambda_2} d\lambda$$

$$[V/m^2] \qquad (2.23)$$

To simplify the equations that follow, we may normalize the detected incidance with respect to the parameters of the detector (The noise voltage, the specific detectivity evaluated in the upper wavelength limit, the detector area, and the electrical bandwidth) and some instrument parameters (transmission loss factor and the subtended solid angle). Their product is independent of temperature and wavelength. Working with such normalization value, we can multiply the radiation quantities with the actual values of the parameters to determine the specific performance.

We define the normalized detected incidance to include only the radiative quantities.

$$E^{Dn}_{[\lambda 1,\lambda 2]}(T) = \frac{E^{D}_{[\lambda 1,\lambda 2]}(T)}{\frac{V_n D^*_2(T_D,\lambda_2)}{\sqrt{A_D \Delta f}}\omega\tau} = \frac{c_1}{\pi\lambda_2}\int_{\lambda 1}^{\lambda 2}\frac{1}{\lambda^4}\frac{\varepsilon(T,\lambda)}{\left(\exp(\frac{c_2}{\lambda T})-1\right)}d\lambda$$

$$[W/sr\ m^2] \qquad (2.24)$$

The normalization constant k_D is

$$k_D = \frac{V_n D^*_2(T_D,\lambda_2)}{\sqrt{A_D \Delta f}}\omega\tau \qquad [V\ sr/W] \qquad (2.25)$$

While the emissivity in general depends on wavelength, it usually varies slowly in the specific infrared wavelength interval permitting us to neglect its spectral dependence. The value to take for the emissivity is then the value at the averaged wavelength. We adopt the notation such that line over the physical quantity indicates the average. Then, we can take the emissivity out the integral to obtain a simplified expression for the detected incidance.

$$E^{Dn}_{[\lambda 1,\lambda 2]}(T) = \frac{c_1 \varepsilon(T,\bar{\lambda})}{\pi \lambda_2} \int_{\lambda 1}^{\lambda 2} \frac{1}{\lambda^4} \frac{1}{\left[\exp(\frac{c_2}{\lambda T}) - 1\right]} d\lambda \qquad [\text{W/sr m}^2] \qquad (2.26)$$

We may represent the integral like those in Eq. (2.26) as *I* with a double subscript. The numerical subscripts have the following significance: the first one is the absolute value of the exponent of the wavelength; the second one is the absolute value of the exponent of the square bracket.

Then Eq. (2.26) becomes

$$E^{Dn}_{[\lambda 1,\lambda 2]}(T) = \frac{c_1 \varepsilon(T,\bar{\lambda})}{\pi \lambda_2} I_{41}(\lambda, T) \qquad [\text{W/sr m}^2] \qquad (2.27)$$

We now evaluate $I_{41}(\lambda,T)$

$$I_{41}(\lambda, T) = \int_{\lambda 1}^{\lambda 2} \frac{1}{\lambda^4} \frac{1}{\left[\exp(\frac{c_2}{\lambda T}) - 1\right]} d\lambda \qquad (2.28)$$

The various forms of Planck's equation are usually solved changing the variable replacing the reciprocal of the wavelength with the dimensionless variable *x*, und employing infinite series. The purpose of the change of variable is to allow the integration *by parts*. We prefer to integrate directly in order to maintain the cognizance of the physical quantities. We use the following infinite series to expand the square bracket [7,8]:

$$\sum_{m=1}^{\infty} \alpha^m = \frac{\alpha}{1-\alpha} = \frac{1}{\alpha^{-1}-1} \tag{2.29}$$

Therewith, Eq. (2.28) becomes

$$I_{41}(\lambda,T) = \int_{\lambda 1}^{\lambda 2} \frac{1}{\lambda^4} \sum_{m=1}^{\infty} \exp(-\frac{c_2}{\lambda T})^m d\lambda \tag{2.30}$$

The negative argument of the exponential assures the series convergence.

Now, we realize that the integration and summation are equivalent operations: their order may be interchanged because the wavelength λ and the integer *m* are mutually independent variables.

$$I_{41}(\lambda,T) = \sum_{m=1}^{\infty} \int_{\lambda 1}^{\lambda 2} \frac{exp(-\frac{c_2}{\lambda T})^m}{\lambda^4} d\lambda \tag{2.31}$$

We prefer to evaluate the integral directly upon completing the integrand to make a perfect differential. To accomplish this, we rely on the following identity: we may use of the derivative of the product of an exponential with any function.

$$\frac{d}{d\lambda}\left(e^{g(\lambda)} f(\lambda)\right) = e^{g(\lambda)} \frac{d}{d\lambda}\left(f(\lambda)\right) + e^{g(\lambda)} f(\lambda) \frac{d}{d\lambda}\left(g(\lambda)\right) = e^{g(\lambda)} \left\{ \frac{d}{d\lambda}\left(f(\lambda)\right) + f(\lambda) \frac{d}{d\lambda}\left(g(\lambda)\right) \right\} \tag{2.32}$$

In order to obtain the perfect differential integrand of Eq. (2.31) we will give it the form of the right side of Eq. (2.32). We identify the function $g(\lambda)$ from Eq. (2.31) as $(-mc_2/\lambda T)$, and we find its derivative.

$$\frac{dg(\lambda)}{d\lambda} = \frac{mc_2}{\lambda^2 T} \tag{2.33}$$

Now, we can rewrite $I_{41}(\lambda,T)$ in terms of $g(\lambda)$ and its derivative.

$$I_{41}(\lambda,T) = \sum_{m=1}^{\infty} \int_{\lambda 1}^{\lambda 2} [\exp(g(\lambda))] \left[\frac{1}{\lambda^2} \frac{T}{mc_2} \frac{dg(\lambda)}{d\lambda} \right] d\lambda \tag{2.34}$$

Here we used Eq. (2.33) to define a new function $h(\lambda)$.

$$\frac{T}{mc_2} \frac{dg(\lambda)}{d\lambda} = \frac{1}{\lambda^2} = h(\lambda) \tag{2.35}$$

We need to find $f(\lambda)$ such that the square bracket in Eq. (2.34) is equal to the curly bracket in Eq. (2.32). By construction, referring to each constructed function $fc_i(\lambda)$, where i refers to the reconstructed term.

$$\frac{1}{\lambda^2} \frac{T}{mc_2} \frac{dg(\lambda)}{d\lambda} = \frac{d}{d\lambda}(f(\lambda)) + f(\lambda) \frac{d}{d\lambda}(g(\lambda)) \tag{2.36}$$

From here, we can see the first term of the construction of $f(\lambda)$ as

$$fc_1(\lambda) = \frac{1}{\lambda^2} \frac{T}{mc_2} \tag{2.37}$$

We calculate the derivative of this function.

$$\frac{d}{d\lambda}\left(fc_1(\lambda)\right) = \frac{-2}{\lambda^3}\frac{T}{mc_2} \tag{2.38}$$

Now we add and subtract this derivative inside the square bracket of Eq. (2.34)

$$I_{41}(\lambda,T) = \sum_{m=1}^{\infty}\int_{\lambda 1}^{\lambda 2}\left[\exp(g(\lambda))\right]\left[\frac{1}{\lambda^2}\frac{T}{mc_2}\frac{dg(\lambda)}{d\lambda} - \frac{2}{\lambda^3}\frac{T}{mc_2} + \frac{2}{\lambda^3}\frac{T}{mc_2}\right]d\lambda \tag{2.39}$$

The expression given by Eq. (2.35) may be substituted in the last term of Eq. (2.39).

Then we factor *h(λ)* from the first and third term.

$$I_{41}(\lambda,T) = \sum_{m=1}^{\infty}\int_{\lambda 1}^{\lambda 2}\left[exp(g(\lambda))\right]\left[\left(\frac{1}{\lambda^2} + \frac{2}{\lambda}\frac{T}{m.c_2}\frac{dg(\lambda)}{d\lambda}\right)\frac{T}{mc_2}\frac{d}{d\lambda}\left(g(\lambda)\right) - \frac{2}{\lambda^3}\frac{T}{mc_2}\right]d\lambda \tag{2.40}$$

From this equation we identify the second term in the reconstruction of *f(λ)*.

$$fc_2(\lambda) = \frac{2}{\lambda}\left(\frac{T}{mc_2}\right)^2 \tag{2.41}$$

Its derivative

$$\frac{d}{d\lambda}\left(fc_2(\lambda)\right) = \frac{-2}{\lambda^2}\left(\frac{T}{mc_2}\right)^2 \tag{2.42}$$

Again, we add and subtract this derivative inside the square bracket of (2.39)

$$I_{41}(\lambda,T) = \sum_{m=1}^{\infty}\int_{\lambda 1}^{\lambda 2}\left[\exp(g(\lambda))\right]\left[\left(\frac{1}{\lambda^2}+\frac{2}{\lambda}\frac{T}{mc_2}\frac{dg(\lambda)}{d\lambda}\right)\frac{T}{mc_2}\frac{d}{d\lambda}\left(g(\lambda)\right) - \frac{2}{\lambda^3}\frac{T}{mc_2} - \frac{2}{\lambda^2}\left(\frac{T}{mc_2}\right)^2 + \frac{2}{\lambda^2}\left(\frac{T}{mc_2}\right)^2\right]d\lambda \tag{2.43}$$

We factor out the function *h(λ)* from the first and fourth term, again using Eq. (2.35).

$$I_{41}(\lambda,T) = \sum_{m=1}^{\infty}\int_{\lambda 1}^{\lambda 2}\left[\exp(g(\lambda))\right]\left[\left(\frac{1}{\lambda^2}+\frac{2}{\lambda}\frac{T}{mc_2}+2\left(\frac{T}{mc_2}\right)^2\right)\frac{T}{mc_2}\frac{d}{d\lambda}\left(g(\lambda)\right) - \frac{2}{\lambda^3}\frac{T}{mc_2} - \frac{2}{\lambda^2}\left(\frac{T}{mc_2}\right)^2\right]d\lambda \tag{2.44}$$

The third term of the construction of *f(λ)* is then identified as

$$fc_3(\lambda) = 2\left(\frac{T}{mc_2}\right)^3 \tag{2.45}$$

Because the derivative of Eq. (2.45) is zero, the process has ended, and the function has been found. Finally, we can write out the complete function *f(λ)* using the terms given in Eqs. (2.37), (2.41), and (2.45).

$$f(\lambda) = \left(\frac{1}{\lambda^2}+\frac{2}{\lambda}\frac{T}{mc_2}+2\left(\frac{T}{mc_2}\right)^2\right)\frac{T}{mc_2} \tag{2.46}$$

Then, the derivative of the function $f(\lambda)$ is

$$\frac{d}{d\lambda}\left(f(\lambda)\right)=\left(\frac{2}{\lambda^3}\frac{T}{mc_2}-\frac{2}{\lambda^2}\left(\frac{T}{mc_2}\right)^2\right) \tag{2.47}$$

Using Eq. (2.46) and (2.47) we can solve the integral of Eq. (2.44) because it has the form of Eq. (2.32).

$$I_{41}(T)=\sum_{m=1}^{\infty}\exp\left(\frac{-mc_2}{\lambda T}\right)\left(\frac{1}{\lambda^2}+\frac{2}{\lambda}\frac{T}{mc_2}+2\left(\frac{T}{mc_2}\right)^2\right)\frac{T}{mc_2}\Bigg|_{\lambda=\lambda 1}^{\lambda 2} \tag{2.48}$$

We may replace Eq. (2.48) with Eq. (2.27) to obtain the normalized detected incidance.

$$E_{[\lambda 1,\lambda 2]}^{Dn}(T)=\frac{c_1\varepsilon(T,\bar{\lambda})}{\lambda_2}\frac{T}{c_2}\sum_{m=1}^{\infty}\frac{1}{m}\exp\left(\frac{-mc_2}{\lambda T}\right)\left(\frac{1}{\lambda^2}+\frac{2}{\lambda}\frac{T}{mc_2}+2\left(\frac{T}{mc_2}\right)^2\right)\Bigg|_{\lambda=\lambda 1}^{\lambda 2}$$

$$[\text{W/sr m}^2] \tag{2.49}$$

We multiply out the first term and find out the analytical solution to the series. The last two terms have faster convergence due to higher powers of *m* in denominator.

$$E_{[\lambda 1,\lambda 2]}^{Dn}(T)=\frac{c_1\varepsilon(T,\bar{\lambda})}{\lambda_2}\frac{T}{c_2}\left\{-\frac{1}{\lambda^2}\ln\left[1-\exp\left(\frac{-c_2}{\lambda T}\right)\right]+\right.$$

$$\left.\sum_{m=1}^{\infty}\frac{1}{m}\exp\left(\frac{-mc_2}{\lambda T}\right)\left(\frac{2}{\lambda}\frac{T}{mc_2}+2\left(\frac{T}{mc_2}\right)^2\right)\right\}\Bigg|_{\lambda=\lambda 1}^{\lambda 2}\quad[\text{W/sr m}^2] \tag{2.50}$$

Fig. 2.6 shows the normalized incidance of a tungsten thermal source in two-wavelength interval, [3-5 μm] and [8-14 μm], as function of temperature, detected with a quantum detector.

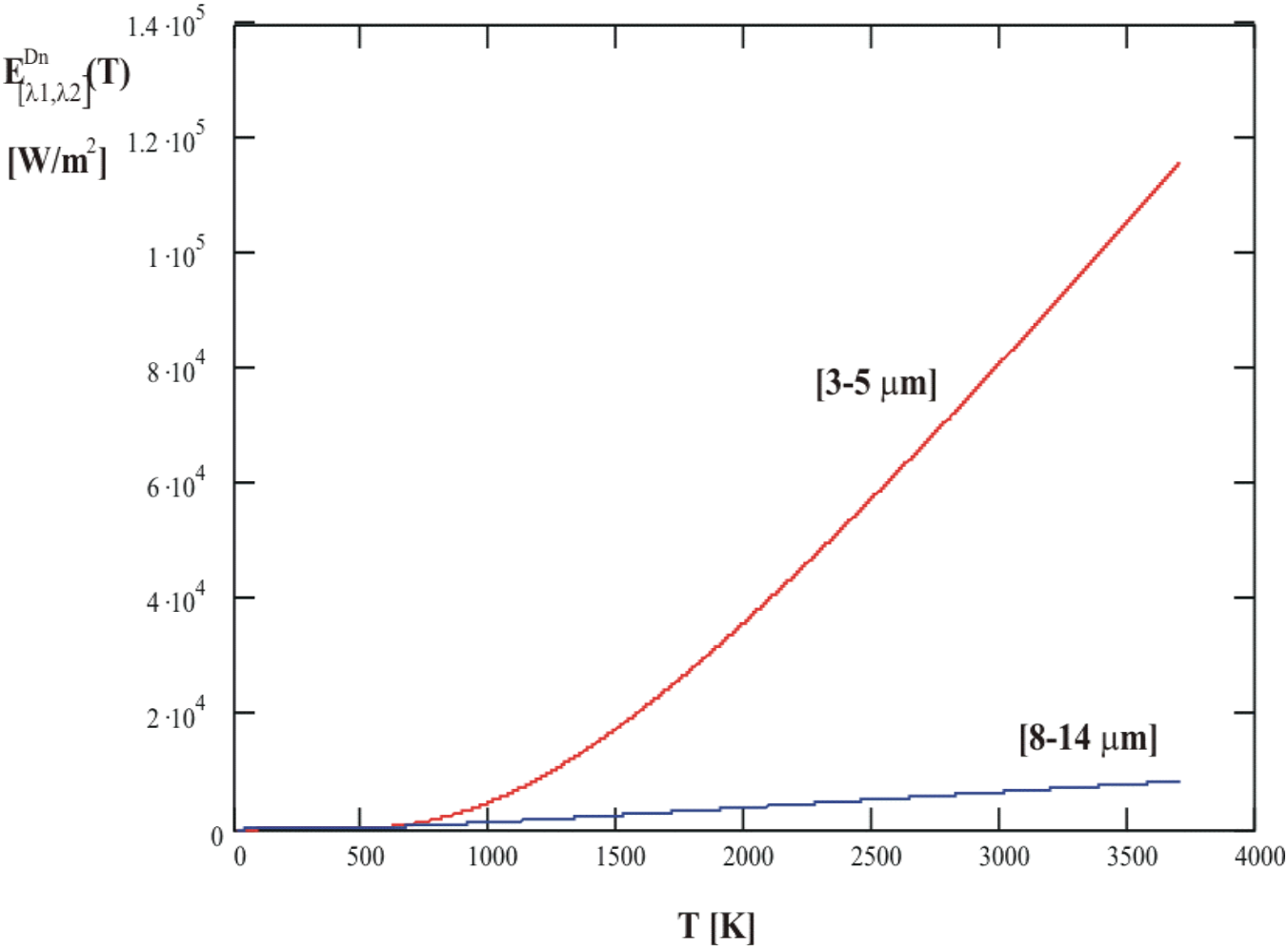

Fig. 2.6 The normalized incidance of a tungsten thermal source in a wavelength interval detected with an ideal quantum detector.

2.4.2 Ideal thermal detector

We may use Eq. (2.7) and Eq. (2.21) to calculate the incidance detected with a thermal detector.

$$E^{D}_{[\lambda 1,\lambda 2]}(T) = c_1 \omega \tau \int_{\lambda 1}^{\lambda 2} \frac{1}{\lambda^5} \frac{\varepsilon(T,\lambda)}{\exp\left(\frac{c_2}{\lambda T}\right) - 1} \frac{D^*(T_D) V_n}{\sqrt{A_D \Delta f}} d\lambda \qquad [\mathrm{V/m^2}] \qquad (2.51)$$

The responsivity is independent of the wavelength for an ideal thermal detector; thus, the normalized incidance detected with a thermal detector is

$$E^{Dn}_{[\lambda 1,\lambda 2]}(T) = \frac{E^{D}_{[\lambda 1,\lambda 2]}(T)}{R(T_D,\lambda)\omega\tau} = c_1 \int_{\lambda 1}^{\lambda 2} \frac{1}{\lambda^5} \frac{\varepsilon(T,\lambda)}{\exp\left(\frac{c_2}{\lambda T}\right) - 1} d\lambda \ \ [\mathrm{W/sr.m^2}] \qquad (2.52)$$

We may simplify Eq. (2.51) following the arguments given for Eq. (2.26).

$$E^{Dn}_{[\lambda 1,\lambda 2]} = c_1 \varepsilon(T,\bar{\lambda}) \int_{\lambda 1}^{\lambda 2} \frac{1}{\lambda^5} \frac{1}{\exp\left(\frac{c_2}{\lambda T}\right) - 1} d\lambda \qquad [\mathrm{W/sr\ m^2}] \qquad (2.53)$$

We may write this equation succinctly using the same notation as previously.

$$E^{Dn}_{[\lambda 1,\lambda 2]} = c_1 \varepsilon(T,\bar{\lambda}) I_{51}(\lambda,T) \qquad [\mathrm{W/sr\ m^2}] \qquad (2.54)$$

The integral $I_{51}(\lambda,T)$ is defined as

$$I_{51}(\lambda,T) = \int_{\lambda 1}^{\lambda 2} \frac{1}{\lambda^5} \frac{1}{exp\left(\frac{c_2}{\lambda T}\right) - 1} d\lambda \qquad (2.55)$$

We expand this integral using the summation in Eq. (2.29).

$$I_{51}(\lambda,T) = \int_{\lambda 1}^{\lambda 2} \lambda^{-5} \sum_{m=1}^{\infty} exp(-c_2 / \lambda T)^m \, d\lambda \tag{2.56}$$

The order of the two operations may be interchanged, because λ and m are independent variables.

$$I_{51}(\lambda,T) = \sum_{m=1}^{\infty} \int_{\lambda 1}^{\lambda 2} \frac{exp(-c_2 / \lambda T)^m}{\lambda^5} d\lambda \tag{2.57}$$

We may used again the derivative of the product of an exponential with any function to evaluate the integral, as we did with Eq. (2.28). We rewrite $I_{51}(\lambda,T)$ using Eq. (2.33)

$$I_{51}(\lambda,T) = \sum_{m=1}^{\infty} \int_{\lambda 1}^{\lambda 2} exp(g(\lambda) \left[\frac{1}{\lambda^3} \frac{T}{mc_2} \frac{d}{d\lambda} g(\lambda) \right] d\lambda \tag{2.58}$$

Now, we construct the derivative of $f(x)$ and compensate for the added terms.

$$I_{51}(\lambda,T) = \sum_{m=1}^{\infty} \int_{\lambda 1}^{\lambda 2} exp(g(\lambda) \left[\left(\frac{1}{\lambda^3} + \frac{3}{\lambda^2} \frac{T}{mc_2} + \frac{6}{\lambda} \left(\frac{T}{mc_2} \right)^2 + 6 \left(\frac{T}{mc_2} \right)^3 \right) \frac{T}{mc_2} \frac{d}{d\lambda} (g(\lambda)) \right.$$

$$\left. - \frac{3}{\lambda^4} \frac{T}{mc_2} - \frac{6}{\lambda^3} \left(\frac{T}{mc_2} \right)^2 - \frac{6}{\lambda^2} \left(\frac{T}{mc_2} \right)^3 \right] d\lambda \tag{2.59}$$

We have the form proposed in Eq. (2.32), so we may write out the solved integral.

$$I_{51}(\lambda,T) = \sum_{m=1}^{\infty} exp\left(\frac{-mc_2}{\lambda T}\right)\left(\frac{1}{\lambda^3} + \frac{3}{\lambda^2}\frac{T}{mc_2} + \frac{6}{\lambda}\left(\frac{T}{mc_2}\right)^2 + 6\left(\frac{T}{mc_2}\right)^3\right)\frac{T}{mc_2}\Bigg|_{\lambda=\lambda 1}^{\lambda 2} \qquad (2.60)$$

With this result, Eq. (2.54) becomes

$$E_{[\lambda 1,\lambda 2]}^{Dn} = c_1\varepsilon(T,\bar{\lambda})\sum_{m=1}^{\infty}\frac{1}{m}\exp\left(\frac{-mc_2}{\lambda T}\right)\left(\frac{1}{\lambda^3}+\frac{3}{\lambda^2}\frac{T}{mc_2}+\frac{6}{\lambda}\left(\frac{T}{mc_2}\right)^2+6\left(\frac{T}{mc_2}\right)^3\right)\Bigg|_{\lambda=\lambda 1}^{\lambda 2}$$

$$[\mathrm{W/sr\ m^2}] \qquad (2.61)$$

We solve analytically the first term of the summation, remaining three terms. These terms have a faster convergence.

$$E_{[\lambda 1,\lambda 2]}^{Dn}(T) = c_1\varepsilon(T,\bar{\lambda})\frac{T}{c_2}\left\{-\frac{1}{\lambda^3}ln\left[1-exp\left(\frac{-c_2}{\lambda T}\right)\right]+\right.$$

$$\left.\sum_{m=1}^{\infty}\frac{1}{m}exp\left(\frac{-mc_2}{\lambda T}\right)\left(\frac{3}{\lambda^2}\frac{T}{mc_2}+\frac{6}{\lambda}\left(\frac{T}{mc_2}\right)^2+6\left(\frac{T}{mc_2}\right)^3\right)\right\}\Bigg|_{\lambda=\lambda 1}^{\lambda 2}$$

$$[\mathrm{W/sr\ m^2}] \qquad (2.62)$$

Fig. 2.7 shows the normalized incidance of tungsten termal source in two-wavelength interval, [3-5 μm] and [8-14 μm], as a function of temperature, detected with a thermal detector.

This equation may be evaluated in the interval [0,∞].

$$E^{Dn}_{[\lambda 1,\lambda 2]} = c_1 \varepsilon(T,\bar{\lambda}) \frac{6T^4\pi^4}{c_2^4 90} = 2\pi hc^2 \varepsilon(T,\bar{\lambda}) \left(\frac{Tk\pi}{hc}\right)^4 \frac{1}{15} = \varepsilon(T,\bar{\lambda})\sigma T^4 \qquad (2.63)$$

This result agrees with the closed form evaluation (Richtmyer, 1969).

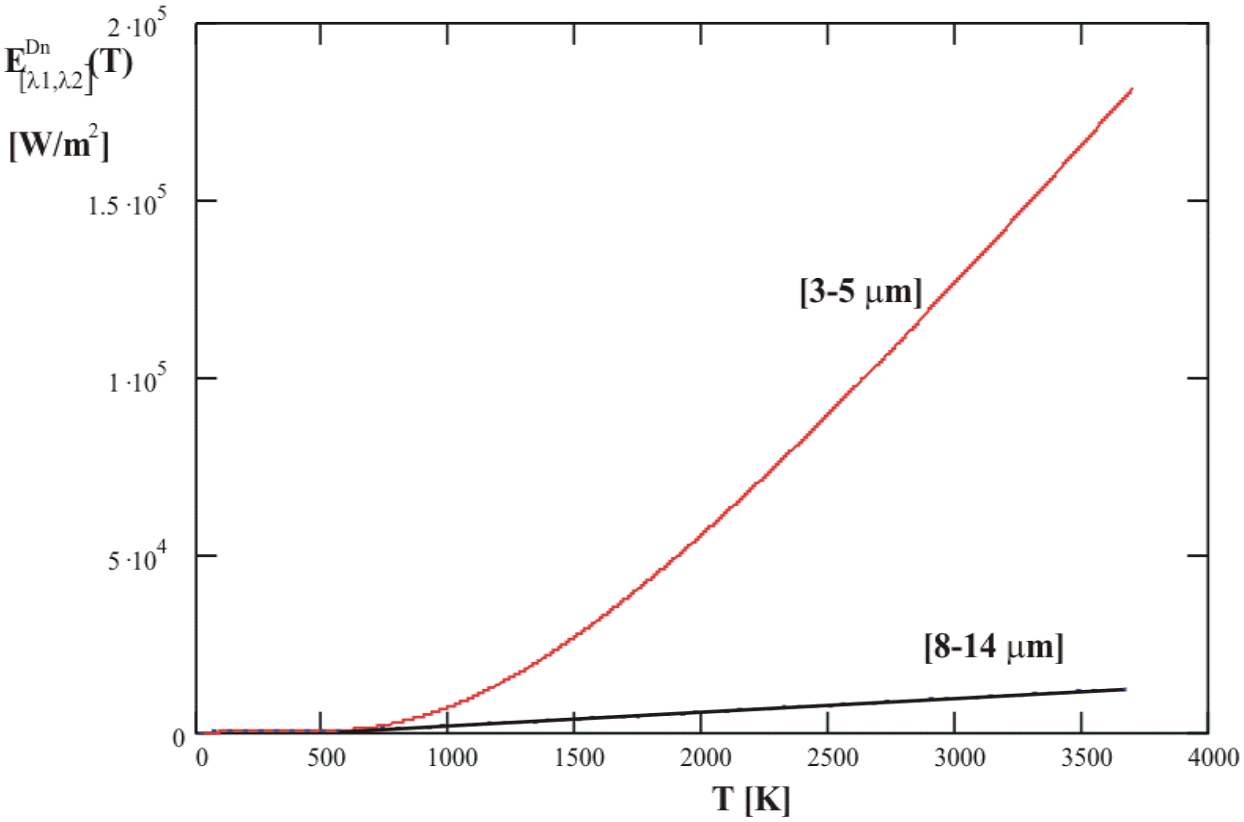

Fig.2.7 The normalized incidance of a tungsten thermal source in a wavelength interval detected with an ideal thermal detector.

2.5 Conclusions

We use the figures of merit to asses the performance of ideal thermal and quantum detectors. We evaluated the total radiation emitted in a wavelength interval, requiring the integration of the Planck's equation. The signal that the detector registers depends on its type, its sensitivity and non-radiometric characteristics. We applied the

result to the tungsten thermal source, a very important calibration source for spectroscopic applications.

References

[1] G. Paez, Infrared signal detection, PhD Thesis, chapter 3,(2000).

[2] M.S. Strojnik, G. Paez, Radiometry, in: D. Malacara, B. Thompson (Eds.), Handbook of Optical Engineering, Marcel Dekker, New York, NY, 2001, pp. 649–700.

[3] G. Paez, M.S. Scholl, Thermal contrast detected with a thermal detector, Infrared Phys. Technol. 40 (1999) 109-116.

[4] G. Paez, M.S. Scholl, Thermal contrast detected with a quantum detector, Infrared Phys. Technol. 40 (1999) 261-265.

[5] F. Nicodemus, self study manual on optical radiation measurements, Part 1, Concepts, Superintendent of Documents, U.S. Government Printing Office, Washington, DC 20402, 1976.

[6] W.L. Wolfe, G.J. Zissis, Infrared Handbook, the radiation Theory, Office of Naval Research. (1978) Chapter 1.

[7] M.S. Scholl, Errors in radiance simulation and scene discrimination, Appl. Opt. 21 (10) (1982) 1839-1843.

[8] M.S. Scholl, Thermal considerations in the design of a dynamic IR source,, Appl. Opt. 21(4) (1982) 660-667.

Chapter 3

Theoretical comparison of thermal contrast detected with thermal and quantum detector

3.1 Introduction

We have previously determined the detected change in incidance at the focal plane of an infrared instrument, integrated over a wavelength interval, arising from the combination of the change in both emissivity and temperature. We propose to call this quantity the detected thermal contrast. This is to differentiate it from the traditional contrast, the term that generally does not consider any detection process, and the thermal contrast, the expression that denotes the change in incident flux at the detector from the radiation of a blackbody source arising from the temperature change [1,2]

We employ the nomenclature propose by Nicodemus [3,4]. Generally the quantum detectors have been recognized as superior in their capability to detect small differences in radiation. However, the numerous advantages of uncooled , thermal detectors in an agricultural environment dictate that their performance be assessed also for remote monitoring of such process. Thus we compare the contrast detected with the modern thermal and quantum detectors used in the focal plane of a radiometer.

3.2 Detected contrast for IR monitoring

We summarize here the pertinent steps leading to the results for the detected thermal contrast. We use the expression, previously derived, for the spectral incidance onto the image plane of an optical system [5].

$$E_\lambda(T) = \omega\tau L_\lambda(T) = \omega\tau(c_1/\pi)\varepsilon(T)\lambda^{-5}\left[e^{c2/\lambda T)} - 1\right]^{-1} \qquad [\mathrm{W/(m^2\mu m)}] \quad (3.1)$$

In this equation, ω is the solid angle subtended by the optical system at the focal plane and τ is the transmittance factor of the intervening media, including the optical system [8,9]. Planck's law gives the spectral radiance of the thermal source $L_\lambda(T)$. In this expression c_1 is the first radiation constant, $2\pi hc^2 = 3.7415 \times 10^8$ W $\mu m^4 m^{-2}$, and c_2 is the second radiation constant, $ch/k = 1.43879 \times 10^4$ μm K. Upon practical considerations and for simplicity, the emissivity, $\varepsilon(T)$, is assumed constant over the wavelength interval $[\lambda_1, \lambda_2]$, specified within the limits of integration. This restricts our analytical results to the gray-body radiators whose emitted radiant power depends only on the source temperature and wavelength-independent emissivity; however the general steps indicated here are applicable to the spectral and line emitters as well.

The detected incidance $E^D_{[\lambda 1,\lambda 2]}(T)$ is that obtained at the output of the detector with the responsivity $\Re(\lambda)$ that integrates the incident radiation over the spectral region of the detector sensitivity. We consider the intervals [*3-5* μm] and [*8-12* μm], the windows of

atmospheric transmission, whose transmission factor τ is largely independent of wavelength.

$$E^{D}_{[\lambda 1,\lambda 2]}(T) = \omega\tau(c_1/\pi)\left\{\varepsilon(T)\int_{\lambda 1}^{\lambda 2}\Re(\lambda)\lambda^{-5}\left[e^{(c2/\lambda T)}-1\right]^{-1}d\lambda\right\} \quad [\mathrm{V/m^2}] \qquad (3.2)$$

Next, we take the derivative of the detected incidance $E^{D}_{[\lambda 1,\lambda 2]}(T)$ with respect to temperature in order to find how the detected incidance changes with temperature. A subscript indicates a derivative with respect to the quantity.

$$E^{D}_{[\lambda 1,\lambda 2]T}(T) = \omega\tau(c_1/\pi)\{\varepsilon_T\int_{\lambda 1}^{\lambda 2}\Re(\lambda)\lambda^{-5}\left[e^{(c2/\lambda T)}-1\right]^{-1}d\lambda + [\varepsilon(T)/T][c_2/T]\int_{\lambda 1}^{\lambda 2}\Re(\lambda)\lambda^{-6}e^{(c2/\lambda T)}\left[e^{(c2/\lambda T)}-1\right]^{-2}d\lambda\} \quad [\mathrm{V/(m^2\cdot K)}] \quad (3.3)$$

The evaluation of these two integrals depends on the detector responsivity function, $\Re(\lambda)$.

3.3. Derivative of the detected incidance in a wavelength interval

Next we consider the specific cases of the thermal and the quantum detectors. The superscripts *T* and *Q* denote with thermal and quantum detectors, respectively.

3.3.1 *Thermal detector*

The responsivity of an ideal thermal detector is independent of wavelength.

$$\Re(\lambda) = \Re_0 = [V_n / \sqrt{A_d \Delta f}\,] D_0^* \qquad \text{[V/W]} \qquad (3.4)$$

In this expression V_n denotes noise voltage, A_d detector area, Δf is the frequency bandwidth of the detector circuit, and D_0^* is the detectivity-star.

Substituting Eq.(3.4) into Eq.(3.3), the wavelength-independent responsivity may be placed outside the integrals. The resulting integrals and derivatives of the blackbody radiance had been evaluated previously [4,8,9]. It is a standard practice to change the variable from λ to x ($x = c_2/\lambda T$). We also have $x_1 = c_2/\lambda_1 T$ and $x_2 = c_2/\lambda_2 T$. It is customary to expand the denominators in series and integrate the expression term by term.

$$E^{DT}_{[\lambda 1,\lambda 2]T}(T) = \omega\tau(c_1/\pi)\Re_0(T/c_2)^4\{\varepsilon_T \Sigma_1 + [\varepsilon(T)/T]\Sigma_3\} \quad \text{[V/(m}^2\text{·K)]} \qquad (3.5)$$

The symbols for the infinite sums Σ_1 and Σ_3 are defined next

$$\Sigma_1 = \sum_{m=1}^{\infty} m^{-4}\{e^{-mx2}\left[(mx_2)^3 + 3(mx_2)^2 + 6(mx_2) + 6\right] - e^{-mx1}\left[(mx_1)^3 + 3(mx_1)^2 + 6(mx_1) + 6\right]\} \qquad (3.6)$$

$$\Sigma_3 = \sum_{m=1}^{\infty} m^{-4}\{e^{-mx2}\left[(mx_2)^4 + 4(mx_2)^3 + 12(mx_2)^2 + 24(mx_2) + 24\right] - e^{-mx1}\left[(mx_1)^4 + 4(mx_1)^3 + 12(mx_1)^2 + 24(mx_1) + 24\right]\} \qquad (3.7)$$

Eq. (3.5) gives the contrast detected by a thermal detector in a wavelength interval. Terms in Eq. (3.5) correspond to the change in emissivity with temperature and to the change in gray-body radiative emission with respect to temperature, respectively.

3.3.2 *Quantum detector*

The responsivity of an ideal quantum detector is proportional to wavelength.

$$\Re(\lambda) = [V_n / \sqrt{A_d \Delta f}\,]D_2^* / \lambda_2)\lambda = \Re'\lambda \qquad \text{[V/W]} \tag{3.8}$$

Here, λ_2 is the detector cut-off wavelength, and D_2^* is the detectivity-star evaluated at the end wavelength, $D^*(\lambda_2)$.

$$E_{[\lambda 1,\lambda 2]T}^{DQ}(T) = \omega\tau(c_1/\pi)(T/c_2)^3\Re'\{\varepsilon_T\Sigma_2 + [\varepsilon(T)/T]\Sigma_4\} \qquad \text{[V/(m}^2\text{K)]} \tag{3.9}$$

The infinite sums Σ_2 and Σ_4 have likewise been evaluated previously [6, 11, 12].

$$\Sigma_2 = \sum_{m=1}^{\infty} m^{-3}\{e^{-mx2}\left[(mx_2)^2 + 2(mx_2) + 2\right] - e^{-mx1}\left[(mx_1)^3 + 2(mx_1) + 2\right]\} \tag{3.10}$$

$$\Sigma_4 = \sum_{m=1}^{\infty} m^{-3}\{e^{-mx2}\left[(mx_2)^3 + 3(mx_2)^2 + 6(mx_2) + 6\right] - e^{-mx1}\left[(mx_1)^3 + 3(mx_1)^2 + 6(mx_1) + 6\right]\} \tag{3.11}$$

Eq.(3.9) gives the contrast generated by a gray-body source detected with a quantum detector in a wavelength interval. Again, two terms in Eq. (3.9) correspond to the contributions due to the change in emissivity with temperature and to the change in gray-body radiative emission with temperature, respectively.

3. 4 Results and discussion

Next, we compare the relative magnitudes of changes in the detected incidance in the wavelength interval due to the change in emissivity and due to the change in the gray-body radiative emission with the temperature. Thus we evaluated the relative contributions of terms in Eq. (3.5) for thermal detector and Eq. (3.9) for the quantum detector. The measured values of emissivity, $\varepsilon(T)$, and its derivative with respect to temperature, $[\Delta\varepsilon/\Delta T]$ would be preferably inserted in Eqs. (3.5) and. (3.9) to asses their relative importance. Unfortunately, they are not available, most likely because of the measurement difficulties and the lack of historical interest.

First we rewrite the analytical results of the previous section in an identical form. The slash is employed to refer to both the quantities related to the thermal and to the quantum detectors. The quantities with the superscript *T* correspond to the infinite sums with subscripts *1* and *3*. The quantities with superscript *Q* correspond to the sums with subscripts *2* and *4*.

$$E^{DT/Q}_{[\lambda 1,\lambda 2]T}(T) = a^{T/Q}(T)\{[\Delta\varepsilon/\Delta T]\Sigma_{1/2} + [\varepsilon(T)/T]\Sigma_{3/4}\} \qquad [\mathrm{V/(m^2K)}] \qquad (3.12)]$$

Here $a^T(T)$ may be found upon comparing Eq.(3.12) with Eq. (3.5).

$$a^T(T) = \omega\tau(c_1/\pi)\Re_0(T/c_2)^4 \qquad (3.13)$$

Similarly $a^Q(T)$ may be found upon comparing Eq.(3.12) with Eq. (3.9).

$$a^Q(T) = \omega\tau(c_1/\pi)(T/c_2)^3\Re' \qquad (3.14)$$

Next, we asses the relative importance of terms in Eq. (3.12). From the curly bracket we factor out the coefficient of the second sum, $[\varepsilon(T)/T]$.

$$E^{DT/Q}_{[\lambda 1,\lambda 2]T}(T) = a^{T/Q}(T)[\varepsilon(T)/T]\{C(\varepsilon,T)\Sigma_{1/2} + \Sigma_{3/4}\} \quad [\mathrm{V/(m^2K)}] \qquad (3.15)$$

Here we introduce the unknown function $C(\varepsilon,T)$ tat includes the emissivity and temperature effects.

$$C(\varepsilon,T) = [\Delta\varepsilon/\Delta T]/[\varepsilon(T)/T] = [\Delta\varepsilon/\varepsilon(T)]/[\Delta T/T] \qquad (3.16)$$

In the second equality, the physical interpretation for the function C becomes apparent: it is the relative change in emissivity over the relative change in temperature. We may find bounds on this function using the well established rule-of thumb: [4] “for the room temperature applications, the change in emissivity of *1%* is about as affective in generating a change in radiance at the sensor as a change in temperature of *1* K”. This

means that the first term is equal to the second term when the change of emissivity of *0.01* corresponds to a change in temperature of *1* K at *300* K. Under these conditions, two terms in Eq. (3.12) are equal.

$$[\Delta\varepsilon / \Delta T] \sum_{1/2} = [\varepsilon(T) / T] \sum_{3/4} \tag{3.17}$$

Upon solving from Eq. (3.17) for the expression that appears on the right side of Eq.(3.16), we substitute it into Eq.(3.16).

$$C(\varepsilon, T) = [\Delta\varepsilon / \Delta T] / [\varepsilon(T) / T] = \Sigma_{3/4} / \Sigma_{1/2} \tag{3.18}$$

The infinite sums and their quotients have been evaluated previously. The sums $\Sigma_{1/2}$ are approximately *10%* to *20%* of the sums $\Sigma_{3/4}$, depending on the interval of detection, the detector type and the temperature. Thus, the second equality in Eq. (3.18) is bounded between *5* and *10*.

The first equality in Eq.(3.18) is equal to $3/\varepsilon(T)$ by the above rule-of-thumb [4]. When $\varepsilon(T)$ is equal to *1*, the first equality is equal to *3*, much less than the right equality. Only when $\varepsilon(T)$ falls between *0.3* and *0.6* is the first equality bounded by *5* and *10*. The rule-of-dumb has apparently been developed when working with materials that have lower emissivity than *1*. The empirical rule-of-thumb confirms the importance of the second term in Eqs. (3.5) and (3.9) at room temperature. The additional finding demonstrated in this

work is that the contribution due to emissivity changes have been some what underestimated even by the practitioners working with empirical rules (by about *50%*).

The emissivity is indeed available as a function of temperature from room temperature to *500* K in the case of metals like steel and aluminum: the measured change of emissivity with temperature is approximately *0.003/*K. This means that the temperature difference of *1* K results in the change in radiative emission corresponding to *0.3K* solely due to emissivity change with temperature. For these two materials, important for infrared mirror surfaces, one may safely conclude that the real change of temperature of *1* K results in the change of the radiative emission equivalent to temperature change of *1.3*K. Thus, neglecting the emissivity term for this materials results in approximately *30%* error.

This result is significant for the analysis of stray light, ghost images, and Narcissus in infrared optical systems, incorporating cooled optics and metal mirrors. In the following subsections, we consider these effects as they apply to the thermal and quantum detectors.

3.4.*1 Thermal detector*

We write out Eq. (3.15) for a thermal detector, using Eq. (3.13).

$$E^{DT}_{[\lambda 1,\lambda 2]T}(T) = \varepsilon(T)\omega\tau(c_1/\pi c_2)\Re_0(T/c_2)^3\{C(\varepsilon,T)\Sigma_1 + \Sigma_3\} \quad [\mathrm{V/(m^2K]} \qquad (3.19)$$

We remember that the temperature in Eq. (3.19) is around room temperature, and the parameter *C* is a slowly varying function whose value is on the order of *1* to *10*, most likely about *3* to *9*.

Figs. 3.1 and 3.2 show the magnitudes of two terms in the curly bracket, $C(\varepsilon,T)\Sigma_1+\Sigma_3$, for the temperature interval between *0* and *40* °C, and the wavelength intervals [*3-5* μm] and [*8-12* μm], respectively. The function *C* is treated as a parameter, with a value between *0* and *10*.

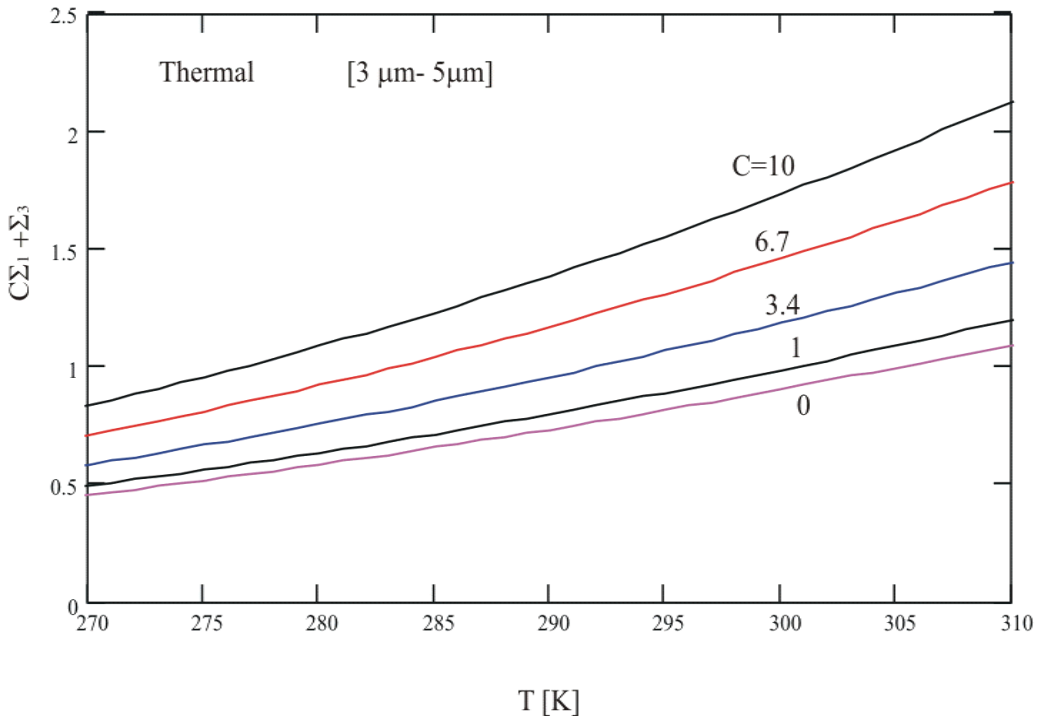

Fig. 3.1 Terms in the curly bracket, $\{C\Sigma_1+\Sigma_3\}$, as a function of temperature between *0* and *40* °C, for the wavelength interval [*3-5* μm]. The function *C* is represented as a parameter, assuming values between *0* and *10*.

The curve with $C = 0$ represents the special case when the emissivity is independent of temperature, the previously treated results. The difference between the $C = 0$ curve and the $C = 1$ shows the value of the infinite sum Σ_1 as a function of temperature. Clearly, the sum is quite small, however the contribution of the first term becomes appreciable when its coefficient is taken into consideration.

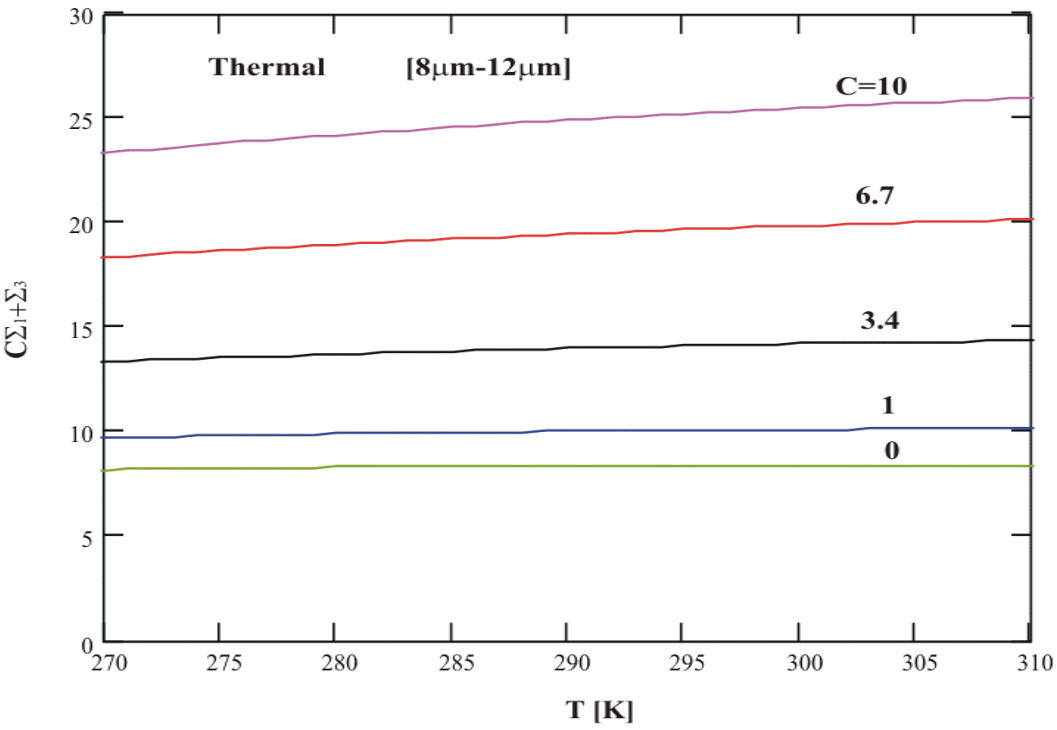

Fig. 3.2 Terms in the curly bracket, $\{C\Sigma_1+\Sigma_3\}$, as a function of temperature between *0* and *40* °C, for the wavelength interval [*8-12* μm]. The function *C* is represented as a parameter, assuming values between *0* and *10*.

3.4.2 *Quantum detector*

Similarly, we write out Eq. (3.15) for a quantum detector, using Eq. (3.14).

$$E^{DQ}_{[\lambda 1,\lambda 2]T}(T) = \varepsilon(T)\omega\tau(c_1/\pi c_2)\Re'(T/c_2)^2\{C(\varepsilon,T)\Sigma_2 + \Sigma_4\} \quad [\mathrm{V/(m^2K]} \qquad (3.20)$$

Again we keep in mind that temperature in Eq. (3.20) is about room temperature, and the parameter *C* is a slowly varying function whose value is on the order of *1* to *10*, most likely

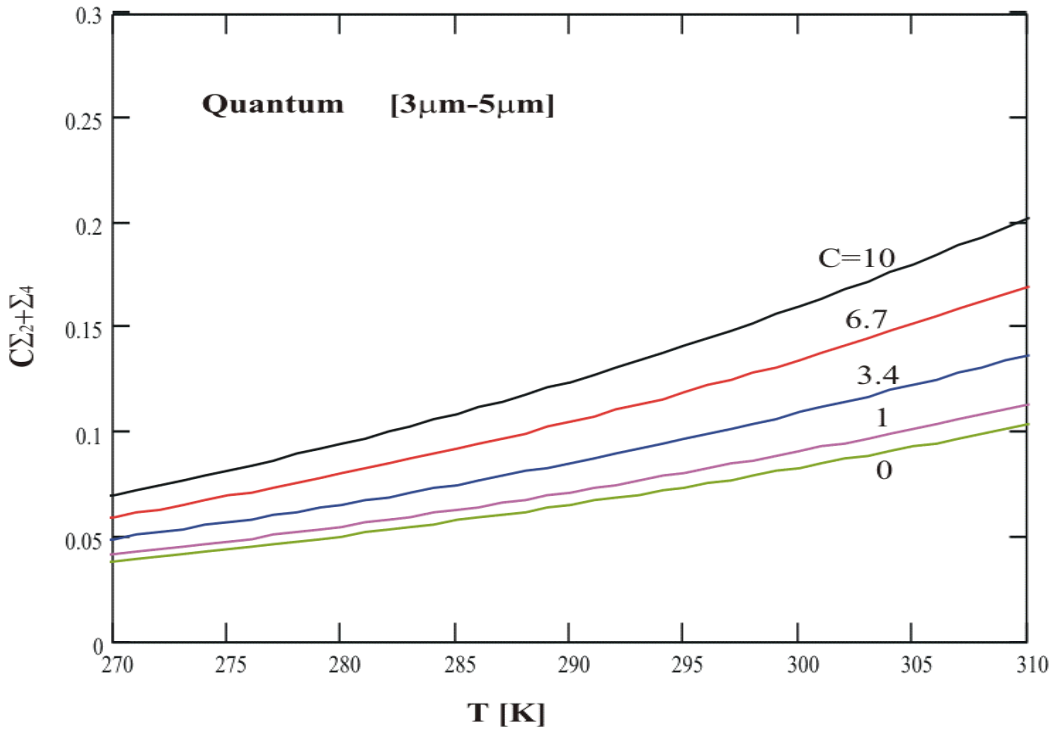

Fig. 3.3 Terms in the curly bracket, $\{C\Sigma_2+\Sigma_4\}$, as a function of temperature between *0* and *40* °C, for the wavelength interval [*3-5* μm]. The function *C* is represented as a parameter, assuming values between *0* and *10*.

about *3* to *9*. Figs. 3.3 and 3.4 show the magnitudes of the two terms in the curly bracket, $C(\varepsilon,T)\Sigma_2+\Sigma_4$, for the temperature interval between *0* and *40* °C, and the wavelength

intervals [*3-5* μm] and [*8-12* μm], respectively. The function *C* is treated as a parameter, with the value between *0* and *10*.

The curve with $C = 0$ represents the special case when the emissivity is independent of temperature, the previously treated results. The difference between the $C = 0$ curve and the $C = 1$ shows the value of the infinite sum Σ_2 as a function of temperature. Clearly, the sum is quite small; however the contribution of the first term becomes appreciable when its coefficient is taken into consideration.

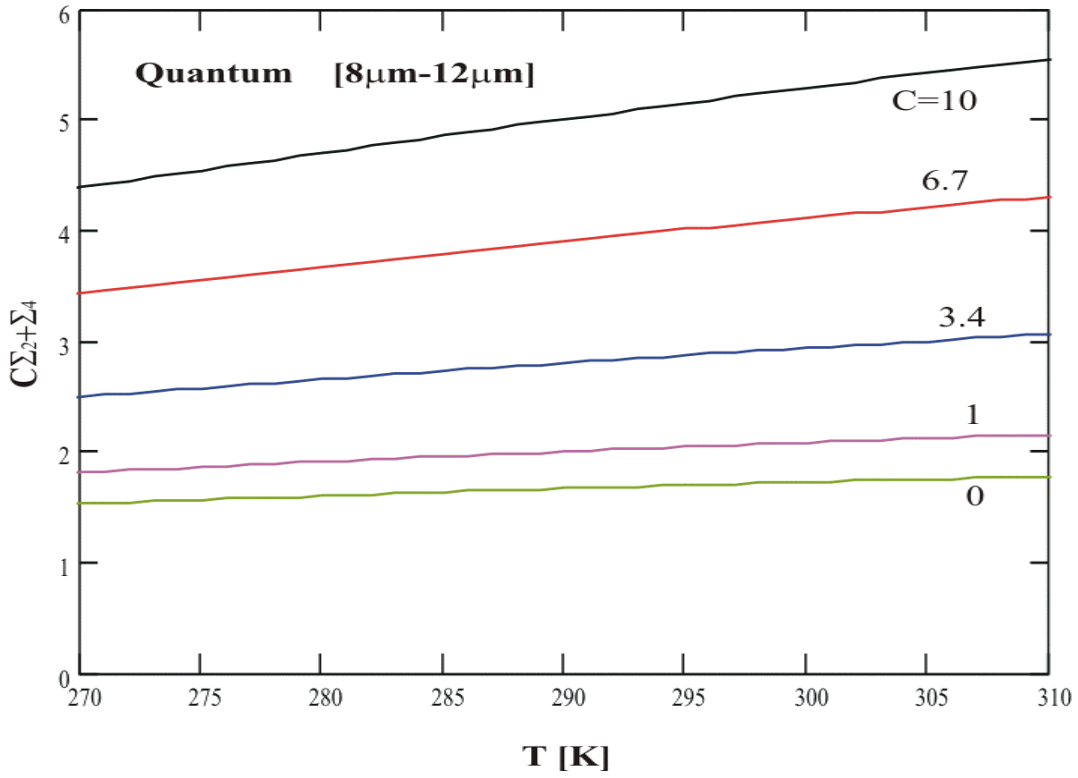

Fig. 3.4 Terms in the curly bracket, $\{C\Sigma_2+\Sigma_4\}$, as a function of temperature between *0* and *40* °C, for the wavelength interval [*8-12* μm]. The function *C* is represented as a parameter, assuming values between *0* and *10*.

3.5. Thermal contrast detected with thermal and quantum detectors: comparison

Next, we simplify the expressions for the radiative incidance (see Eqs. (3.19) and (3.20)) by eliminating the common factors. We define the following expression for the detected thermal contrast, applicable to both the thermal and quantum detectors, $DTC^{T/Q}_{[\lambda 1,\lambda 2]}(T)$.

$$DTC^{T/Q}_{[\lambda 1,\lambda 2]}(T) = \left\{E^{DT/Q}_{[\lambda 1,\lambda 2]T}(T)\right\} / \left\{\varepsilon(T)\omega\tau\left[V_n / \sqrt{A_d \Delta f}\right]\right\} \qquad [\sqrt{Hz}\,/(mK)] \qquad (3.21)$$

Next, we evaluate the detected thermal contrast for the thermal and quantum detectors.

3.5.1 *Thermal detector*

We substitute Eq.(3.13)into Eq. (3.21) to get the detected thermal contrast for the thermal detector.

$$DTC^{T}_{[\lambda 1,\lambda 2]}(T) = (c_1 / \pi c_2) D^*_0 (T / c_2)^3 \{C(\varepsilon, T)\Sigma_1 + \Sigma_3\} \quad [\sqrt{Hz}\,/(mK)] \qquad (3.22)$$

Here we introduce a function $b^T(T)$. It depends on temperature, the detectivity star, D^*_0, and the radiation constants.

$$b^T(T) = (c_1 / c_2 \pi) D^*_0 (T / c_2)^3 \qquad \sqrt{Hz}\,/(mK) \qquad (3.23)$$

Using Eq. (23), Eq. (22) becomes

$$DTC^{T}_{[\lambda 1,\lambda 2]}(T) = b^{T}(T)\{C(\varepsilon,T)\Sigma_1 + \Sigma_3\} \qquad [\sqrt{Hz}\,/(mK)] \qquad (3.24)$$

The published value for D_0^* for a pyrolitic detector at room temperature [4] is 10^9 cm√Hz/(m K). The coefficient b^T (*300* K) evaluated for the room temperature is approximately $4x10^8$ √Hz/(m K).

Figs. 3.5 and 3.6 show the relative detected thermal contrast measured with a thermal detector for the temperature interval between *0* and *40* °C, and the wavelength intervals [*3-5* μm] and [*8-12* μm], respectively. The function *C* is represented as a parameter, with the value between *0* and *10*. As expected, a value an order of magnitude higher for the relative detected contrast is exhibited in the interval with the longer wavelengths.

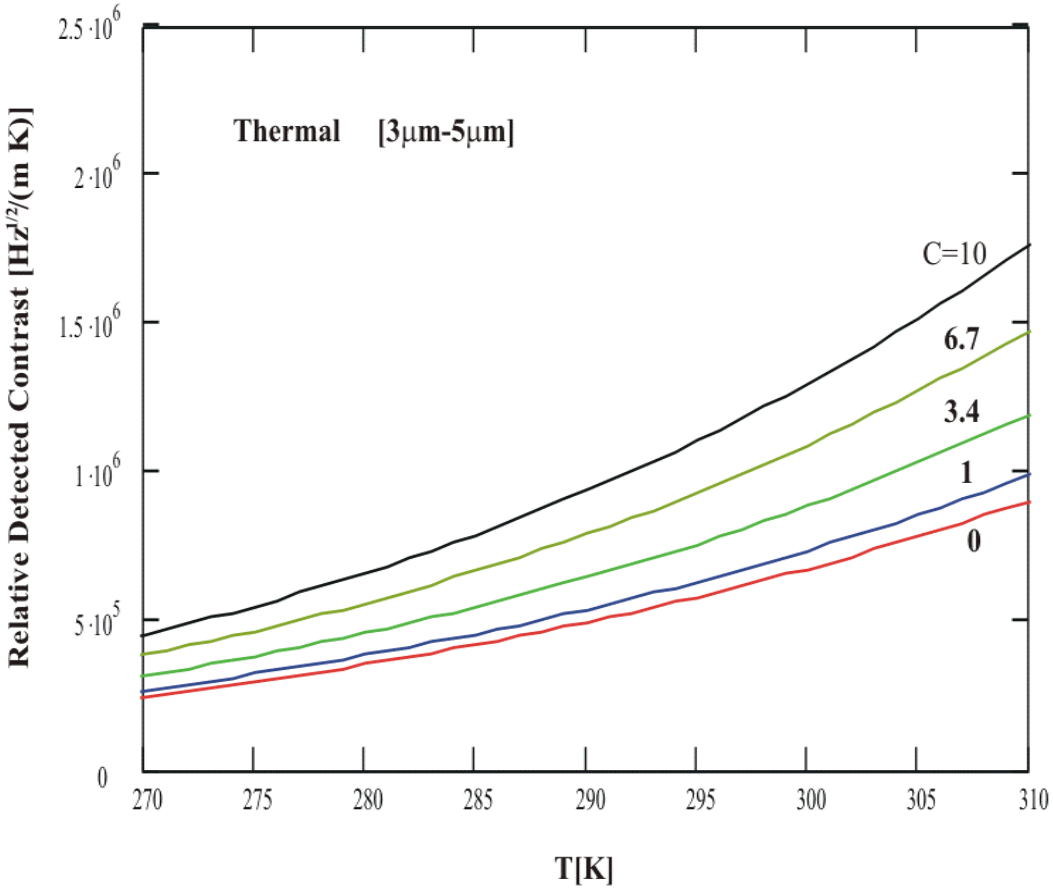

Fig. 3.5 The relative detected thermal contrast obtained with a thermal detector as a function of temperature between *0* and *40* °C, for the wavelength interval [*3-5* μm]. The function *C* is represented as a parameter, assuming values between *0* and *10*.

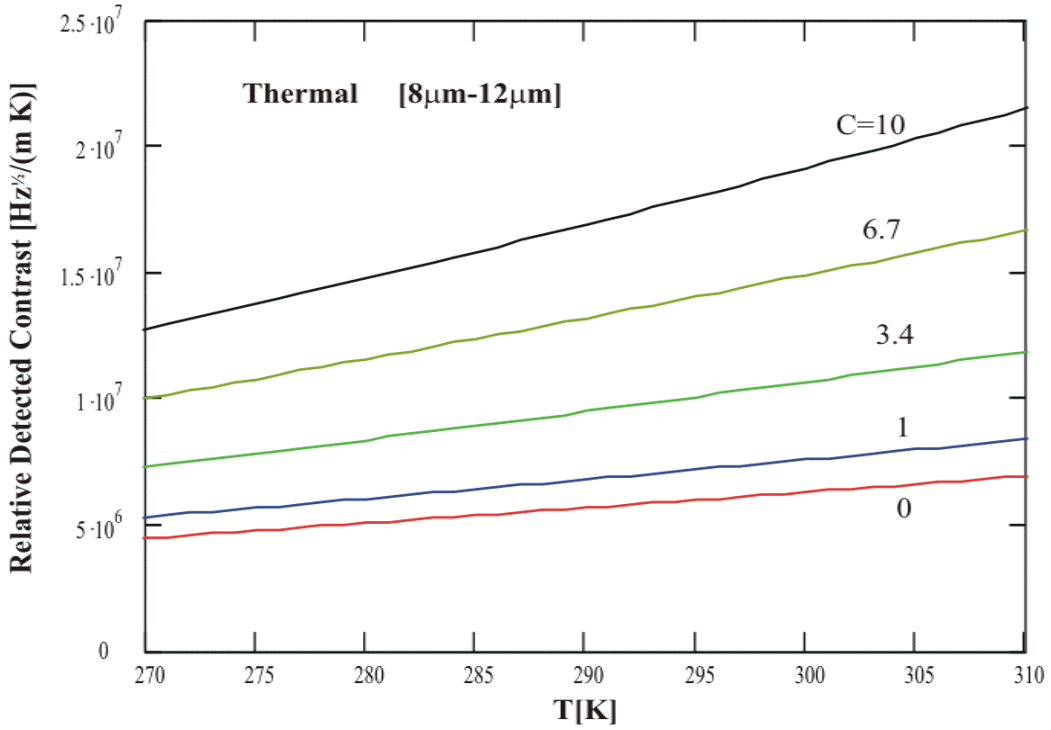

Fig. 3.6 The relative detected thermal contrast obtained with a thermal detector as a function of temperature between *0* and *40* °C, for the wavelength interval [*8-12* μm]. The function *C* is represented as a parameter, assuming values between *0* and *10*.

3.5.2 Quantum detector

Using Eq. (3.14), we write out Eq. (3.21) for a quantum detector

$$DTC^{Q}_{[\lambda 1,\lambda 2]}(T) = (c_1 / \pi c_2)(D^*_2 / \lambda_2)(T / c_2)^2 \{C(\varepsilon, T)\Sigma_2 + \Sigma_4\} \quad [\sqrt{Hz}\,/(mK)] \quad (3.25)$$

Here we introduce a function $b^Q(T)$. It depends on temperature, the detectivity star, D^*_2, the cutoff wavelength, λ_2, and the two radiation constants.

$$b^Q(T) = (c_1 / c_2\pi)D^*_2 / \lambda_2(T / c_2)^2 \qquad [\sqrt{Hz}\,/(mK)] \qquad (3.26)$$

Then Eq. (3.25) becomes

$$DTC^{Q}_{[\lambda 1,\lambda 2]}(T) = b^{Q}(T)\{C(\varepsilon,T)\Sigma_2 + \Sigma_4\} \qquad [\sqrt{Hz}/(mK)] \qquad (3.27)$$

For a cooled HgCdTe detector, the published value for D^*_2 is $3x10^{10}$ cm√Hz/(m K), with the cutoff wavelength of *14* μm [6]. The coefficient b^Q (300K) evaluated for the radiation at ambient temperature is approximately $2x10^8$ √Hz/(m K). Figs. 8 and 9 show the relative detected thermal contrast obtained with a quantum detector, for the temperature interval between *0* and *40* °C, and the wavelength intervals [*3-5* μm] and [*8-12*. μm], respectively. The function *C* is given as a parameter between *0* and *10*. As expected, an order-of-magnitude higher value for the relative detected contrast is exhibited for longer wavelengths.

Figs. 3.9 and 3.10 show the relative thermal contrast detected with a quantum detector, for the following conditions: the value of the parameter *C* is 1, the temperature interval is between *0* and *40* °C, and the wavelength intervals are [*3-5* μm] and [*8-12*. μm]. In both intervals, we note that the quantum detector exhibits approximately *20* times better performance than the thermal one.

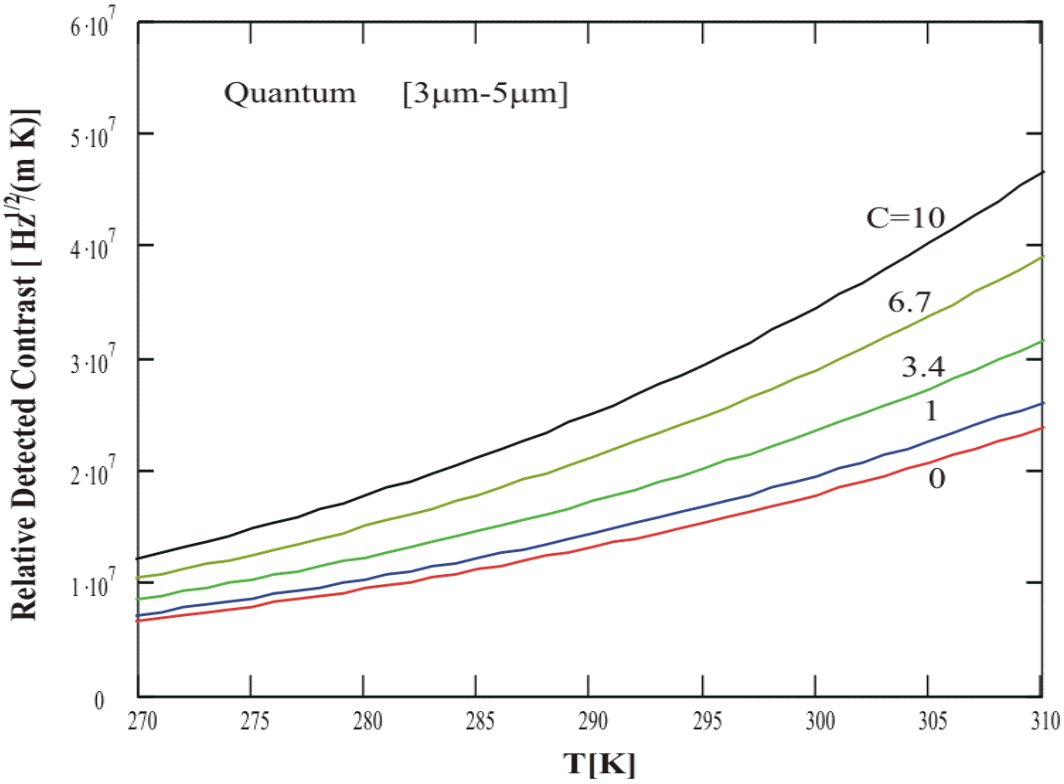

Fig. 3.7 The relative detected thermal contrast obtained with a quantum detector as a function of temperature between *0* and *40* °C, for the wavelength interval [*3-5* μm]. The function *C* is represented as a parameter, assuming values between *0* and *10*.

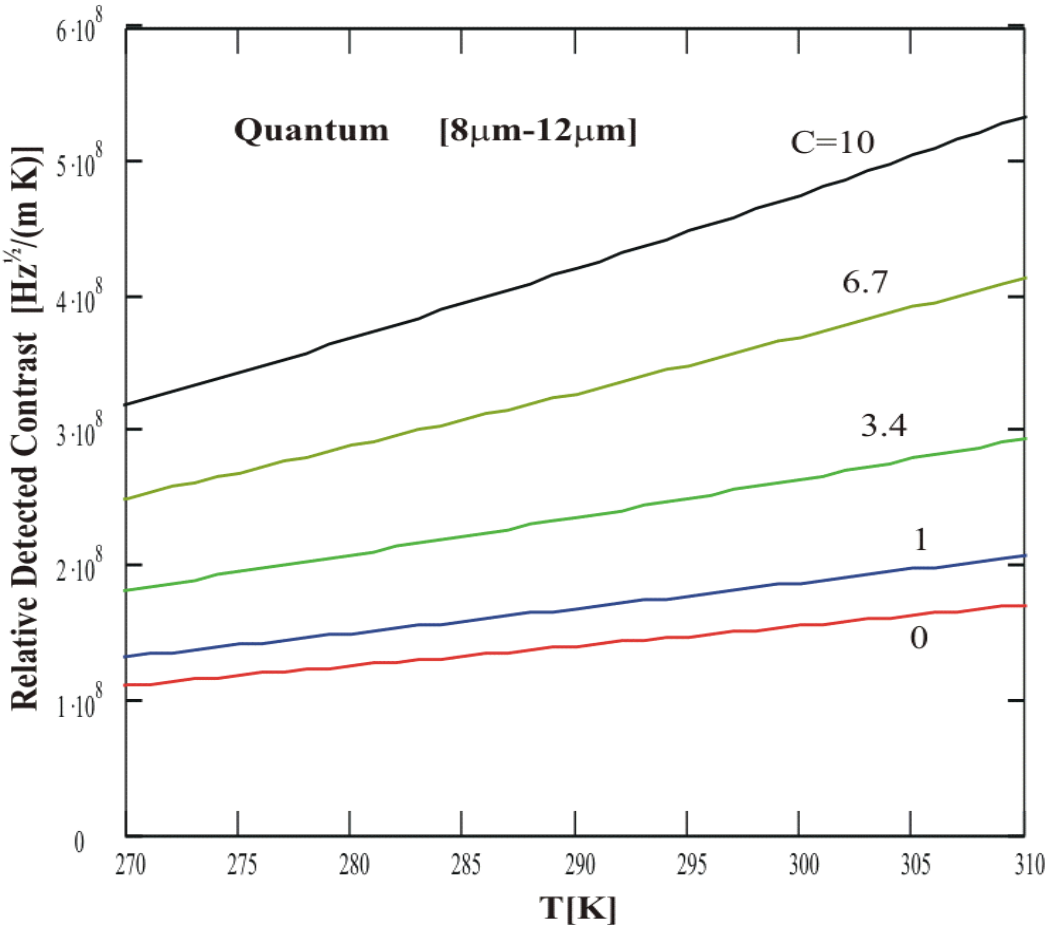

Fig. 3.8 The relative detected thermal contrast obtained with a quantum detector as a function of temperature between *0* and *40* °C, for the wavelength interval [*8-12* μm]. The function *C* is represented as a parameter, assuming values between *0* and *10*.

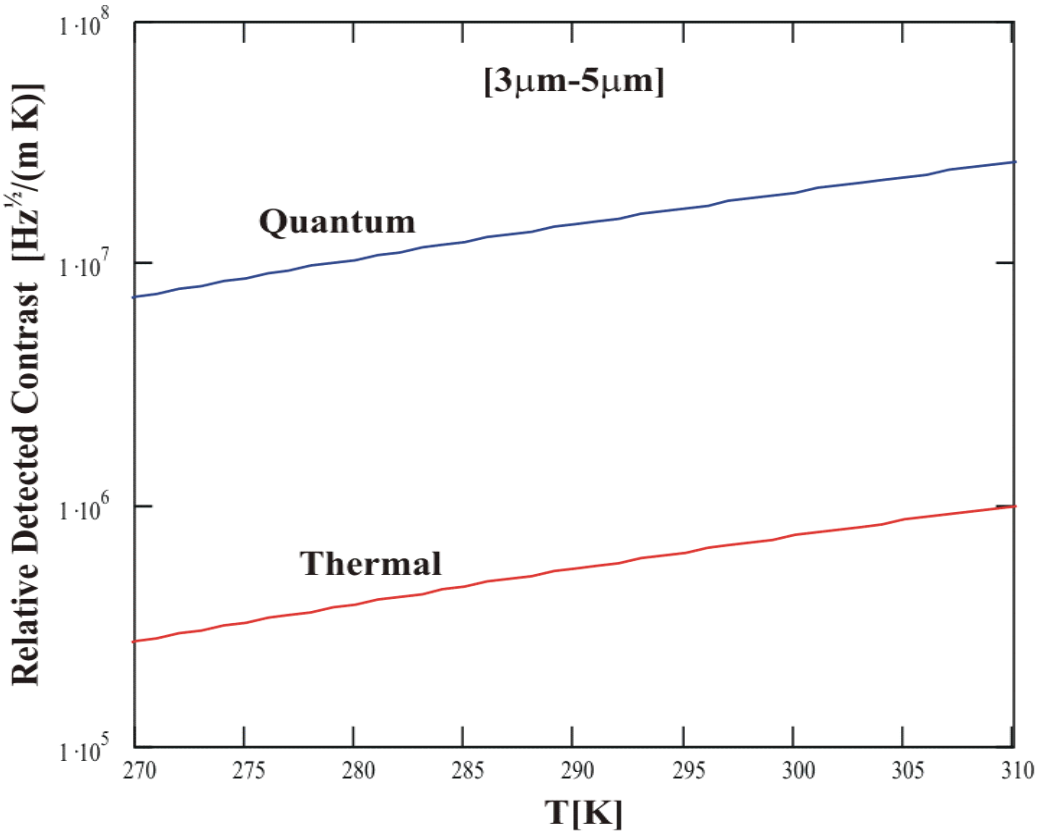

Fig. 3.9 The relative detected thermal contrast obtained with a thermal and quantum detector as a function of temperature between *0* and *40* °C, for the wavelength interval [*3-5* μm]. The parameter *C* is equal to *1*.

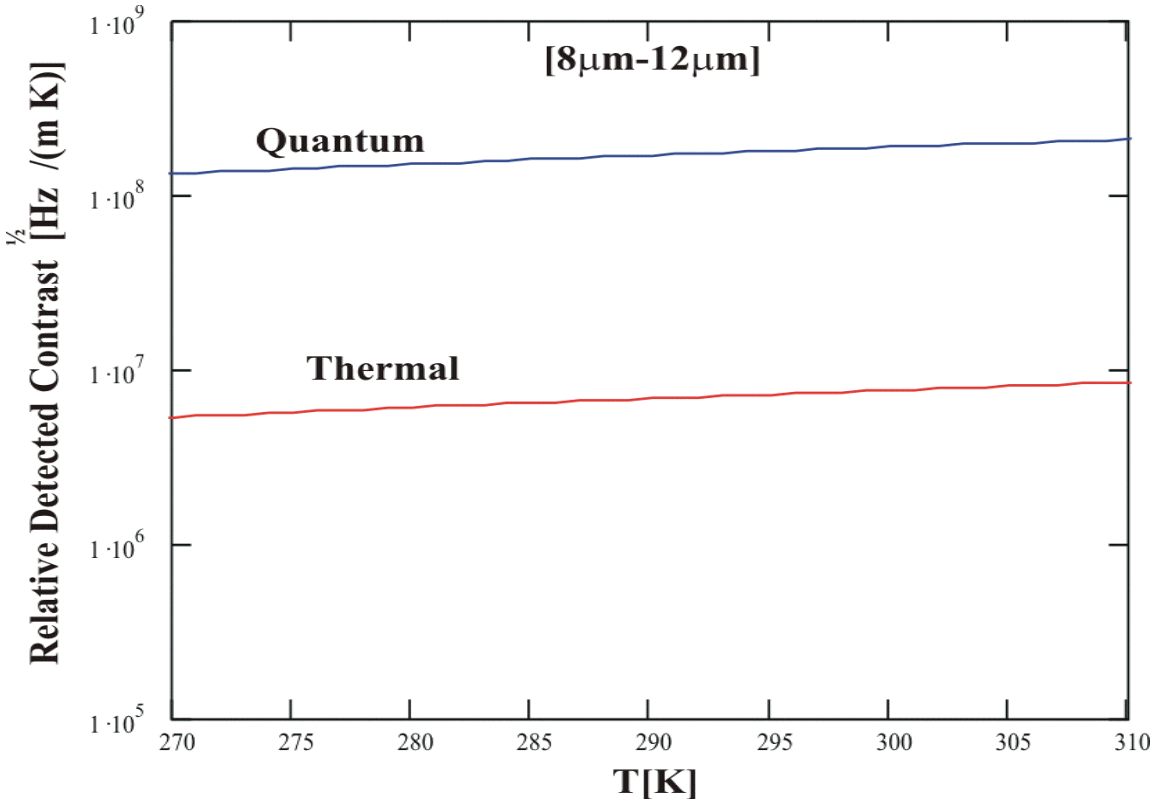

Fig. 3.10 The relative detected thermal contrast obtained with a thermal and quantum detector as a function of temperature between *0* and *40* °C, for the wavelength interval [*8-12* μm]. The parameter *C* is equal to *1*.

3.6 Conclusions

We developed the theoretical expression for the detected thermal contrast detected with the thermal and the quantum detectors in order to perform a reliable comparison and the trade-off analysis between their performances for the routine, remote monitoring of agricultural process. Our analysis includes the contribution to the radiative emission arising from the emissivity change in addition to the traditionally considered one due to temperature change. The former has not been quantified up to now, despite the fact that its contribution has been known. The empirical rule-of-thumb developed by the long-time

practitioner confirms the importance of the second term in Eqs. (3.5) and (3.9) at room temperature. The additional finding demonstrated in this work is that the contribution due to emissivity changes has been underestimated. It introduces about *30%* error for the detected thermal contrast at room temperature.

The detailed contrast evaluations presented here are in general agreement with the previously available qualitative knowledge. Our results confirm that the detected thermal contrast is higher in the [*8-12* μm] wavelength interval than in the [*3-5* μm] interval, independently of the detector type. Similarly, we note that under the same conditions the quantum detector measures *20* times higher detected thermal contrast than the thermal one in either spectral interval, independently of the magnitude of the change of emissivity value.

Thus, we conclude that the quantum detector exhibits better performance than the thermal detector for the remote monitoring of agricultural crops, especially in the case of the urgent need of the early disease detection.

The factor of improvement in the contrast detected with the quantum detector over that with the thermal detector is also about *20* when the detected thermal contrast arises solely due to the change in emissivity. This is significant in the interesting case that the infected plant undergoes only emissivity change without the accompanying change in temperature.

The phenomenon of the detected contrast arising solely due to an emissivity change is particularly relevant to the instrument design, especially for the cooled one, observatory facilities. In such cases, the designer is required to asses future operational performance of an instrument, under unknown conditions of aging in an environment that is not easily predictable or accessible for monitoring. For example, the design studies of the performance for cooled telescopes tend to incorporate the barely achievable, laboratory emissivity values that are likely to deteriorate with time and operational use. The magnitude of the thermal contrast arising solely due to the emissivity term may be determined only when data on emissivity deterioration in-situ, and with use, such as the lifetime data, becomes available.

For the two materials that are important for infrared mirror surface, one may safely conclude that the real change of temperature of *1* K results in a change of the radiative emission equivalent to temperature change of *1.3* K. Thus, neglecting the emissivity term for these materials, it results about an error of *30%* . Further research into application of these results to sources at higher temperatures is in progress [13-15].

References

[1] G. Paez, M.S. Scholl, Thermal contrast detected with a thermal detector, Infrared Phys. Technol. 40 (1999) 109-116.

[2] G. Paez, M.S. Scholl, Thermal contrast detected with a quantum detector, Infrared Phys. Technol. 40 (1999) 261-265.

[3] F. Nicodemus, self study manual on optical radiation measurements, Part 1, Concepts, Superintendent of Documents, U.S. Government Printing Office, Washington, DC 20402, 1976.

[4] W.L. Wolfe, G.J. Zissis, Infrared Handbook, the radiation Theory, Office of Naval Research. (1978) Chapter 1.

[5] M.S. Scholl, G. Paez, Image-plane incidance for a baffled infrared telescope, Infrared Phys. Technol. 38 (10) (1997) 87-92.

[6] M.S. Scholl, Stray light issues for background-limited far infrared telescope operation, Opt. Eng. 33(3) (1994) 681-684.

[7] M.S. Scholl, Design parameters for a two-mirror telescope for stray-ligth, sensitive infrared applications, Infrared Phys. Technol. 37 (1996) 251-257.

[8] M.S. Scholl, Simulation of spectral radiance of a dynamic infrared source, Ph.D. Thesis, The University of Arizona (1979), p.50.

[9] M.S. Scholl, Errors in radiance simulation and scene discrimination, Appl. Opt. 21 (10) (1982) 1839-1843.

[10] M.S. Scholl, Thermal considerations in the design of a dynamic IR source,, Appl. Opt. 21(4) (1982) 660-667.

[11] M.S. Scholl, Spatial and Temporal effects due to target irradiation: a study, Appl. Opt. 21(9) (1982) 1615-1620.

[12] M.S. Scholl, Target temperature distribution generated and maintained by a scanning laser beam, Appl. Opt. 21(12) (1982) 2146-2152.

[13] G. Paez, M.K. Scholl, Evaluation of Er-doped silica as IR-to-visible converter. In: Infrared spaceborne Remote Sensing XII, SPIE Proc. 5543 (2004).

Chapter 4

Two-wavelength differential thermometry for a microscopic extended source

4.1 introduction

Determination of absolute temperature has always been considered a challenging task [1–4]. This is particularly difficult for an extended area sources where small temperature differences may arise upon action of heat transfer mechanisms [5,6]. A tungsten coiled coil source is often used as a reference source in spectrometric reflectance and transmission measurements. In the evaluation of the tungsten source as a calibration standard, we found that the filament temperature actually varies as a function of position, resulting in its radiance variation along position and solid angle. Initially, this appeared contrary to our expectations so we made a significant effort to determine the reasons [7,8].

4.2 Radiative temperature measurements

The initial radiance evaluation over the whole projected coiled coil surface indicated that the structure forms a partially transmissive cavity, increasing the temperature of the inner surface elements. In the second attempt to improve the accuracy of the results, we used a differential two-wavelength thermometry, implemented with the spectrometer. This method was believed to yield more credible results because the only source of error, emissivity differences, is eliminated. The second measurement, described here, provides further verification for the formation of a cavity inside each of the two coils that form the

radiative surface of the tungsten filament. Fig. 4.1 shows a high-resolution image of the filament at 550 nm and with a spectral width of 10 nm. By observing the cavity effects that arise in the tungsten lamp some degree of caution is advised when claiming traceability to the standard sources in the case of microscopic surface elements. We performed a novel temperature measurement in a differential two-wavelength thermometry, in the belief that it was applicable to a microscopic area of the source. Rather than performing a spectroscopy on the same projected surface area of the radiation source, we actually found how the temperature varies along a short line due to microscopic dimensions. Such surface profiles that have likely been measured are outlined in horizontal rectangles, denoted by A, B, C, and D in Fig. 4.1.

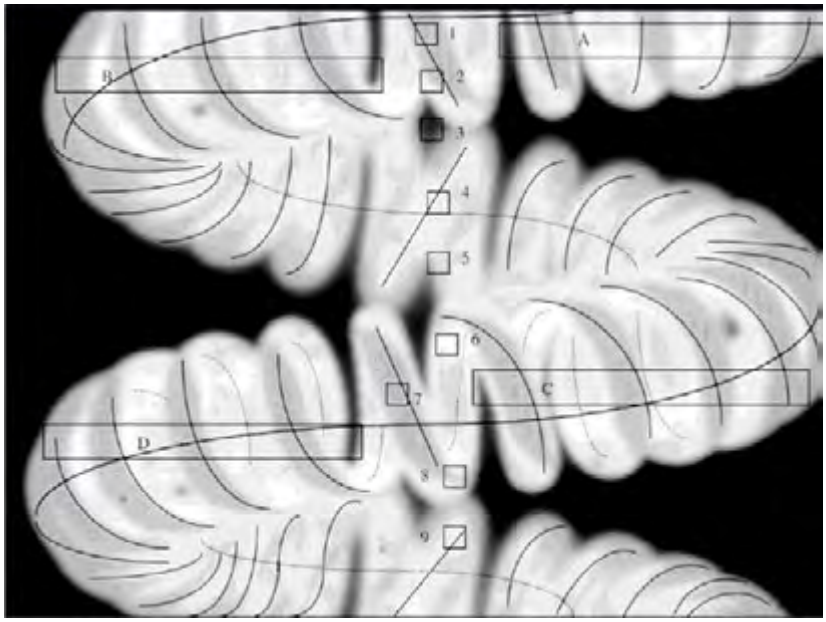

Fig. 4.1. The coiled coil obtained upon imaging on a 2000 x 2000-pixel camera at 550-nm central wavelength and with spectral width of 10 nm. Thin lines are used to enhance the shape of the small diameter coils. In the middle part of the image, the inner surfaces of the small coil are outlined in a thin dotted line, outlining the volume of the small, partially transmitting cavity. Thick lines show the envelope of the large coil with the continuous line indicating the outer surface. The dotted line outlines the inner envelope of the large coil, forming the large porous cavity. Only few surface elements are oriented perpendicular to the line of sight and parallel to the CCD surface, as for example the pixels 1, 4, and 7. Four scans (A, B, C, D) are indicated that could possibly give rise to temperature distribution reported in Fig. 4.6.

4.3 Error evaluation study in digitalization and Wien's approximation.

We can expect an error due the suppressed 1 in the Planck's law. At 2800 K, like in the thermal tungsten source which is a reference source in spectrometric reflectance and transmission measurements. This error become significant as we can see in Fig. 4.2

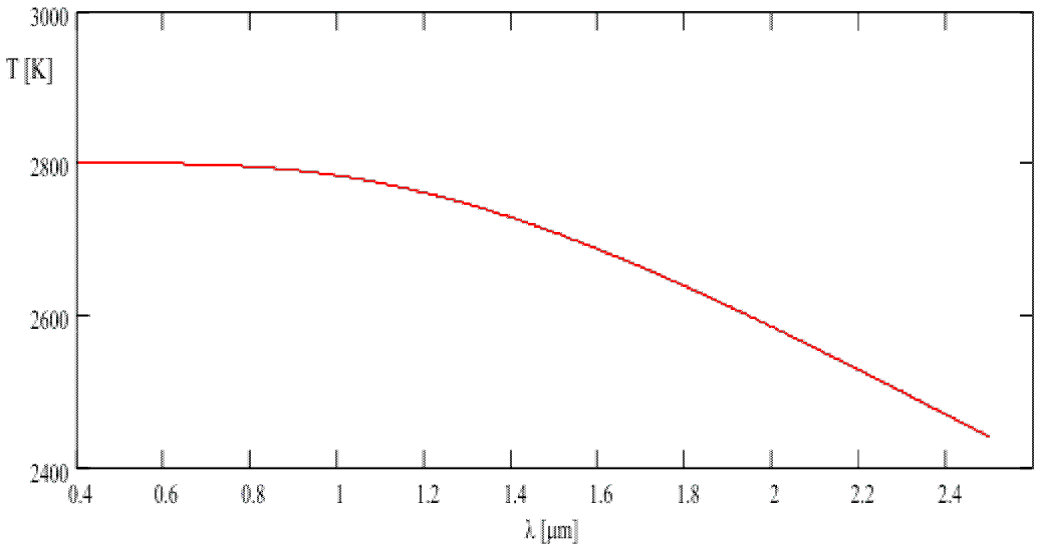

Fig. 4.2. The variation in the calculated temperature due the fact to disregard the one in the Plank's law.

This error increases with the wavelength and with the temperature. Above the 2 μm at the temperature of 2800 K we have more than 8% of error or 217 K, but in 1 μm the error is just 17 K or 0.6%. This is the reason to why we made the select the visible spectral interval 0.4 y 0.8 μm.

Digitalization error. The spectrometer change the analogical signal to a digital one, in this process we can lose some information that can be significant. As the data is taken closer this error will increase due the radiances are very similar, but if the measurements are taken for points that are distant, the emissivity can not be considered as a constant (30nm is an acceptable separation).

We use a 12 bits spectrometer (4096 gray levels), with this device we expect an error of 3% (± 86 K) for measurements taken 0.37 nm apart at the temperature of 2800 K . This error is due to the process of digitalization, Fig. 4.3

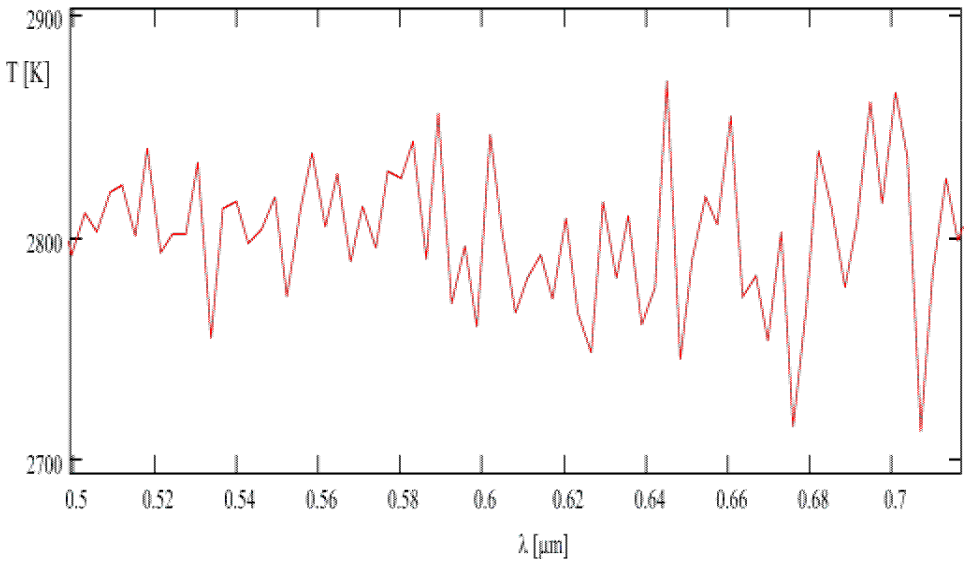

Fig. 4.3 It shows the fluctuation in the calculated temperature due to digitalization with 12 bits at 2800 K.

The same rules applies to different temperatures and wavelengths. In general the error due to suppressed 1 in the Plank's law increases with the wavelength and the temperature. The digitalization error is bigger as the measurements are closer in

wavelength , but the emissivity change with the temperature and with the wavelength, only can be considered constant in short intervals. The emissivity change slowly with the temperature.

4.4 Spectrometry for a microscopic surface element in a tungsten filament

In non-contact temperature measurement, it is implicitly assumed that the surface element is at an specific temperature. Measurement precision is similarly assumed to result in the same value for two consecutive measurements**.** These assumptions may appear to be violated when imaging micro-structures with nanometric precision. As we show next, the averaging rules applied to a macroscopic scale must be applied with caution to micro- and nano-surfaces.

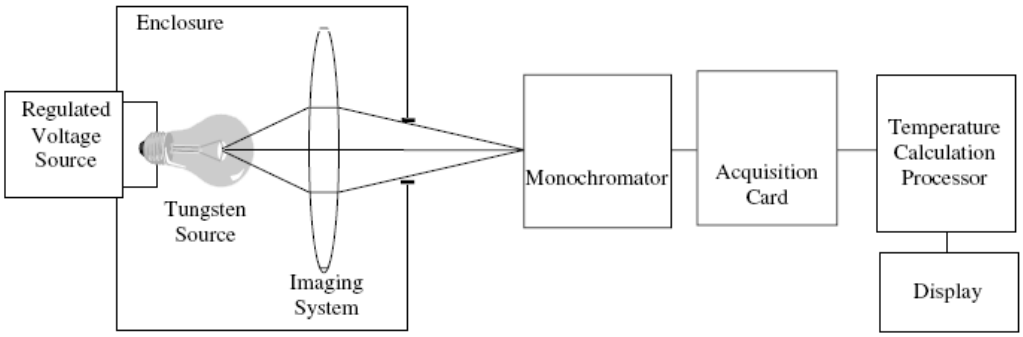

Fig. 4.4 A small area of the tungsten source is imaged on the spectrometer entrance pupil. Temperature is determined continuously as a function of wavelength, using differential two-wavelength thermometry.

Two wavelengths in a spectroscopic setup are separated by 0.3 nm to determine filament temperature of 0.1-mm^2 projected area. Two consecutive measurements may be used for the differential two-wavelength spectrometry. Clearly, any other wavelength pair may also be used for thermometry in macroscopic applications, but not in the microscopic ones. Allowing the spectrometer to record incidance measurements for all wavelengths, temperature may actually be found as a function of wavelength.

A small area (0.1 mm^2) of the tungsten filament is imaged on the spectrometer entrance pupil, as presented schematically in Fig. 4.4. The filament about 4-mm long is placed in the focal plane of the lens with an effective focal distance of 35 mm. The spectrometer entrance pupil is located about 400 mm behind the lens. Filament temperature may be calculated for each pixel, using the familiar two-wavelength thermometry. When two neighboring spectroscopic measurements are used, the emissivity effects may be completely neglected, resulting in the best theoretical measurement, for macroscopic applications.

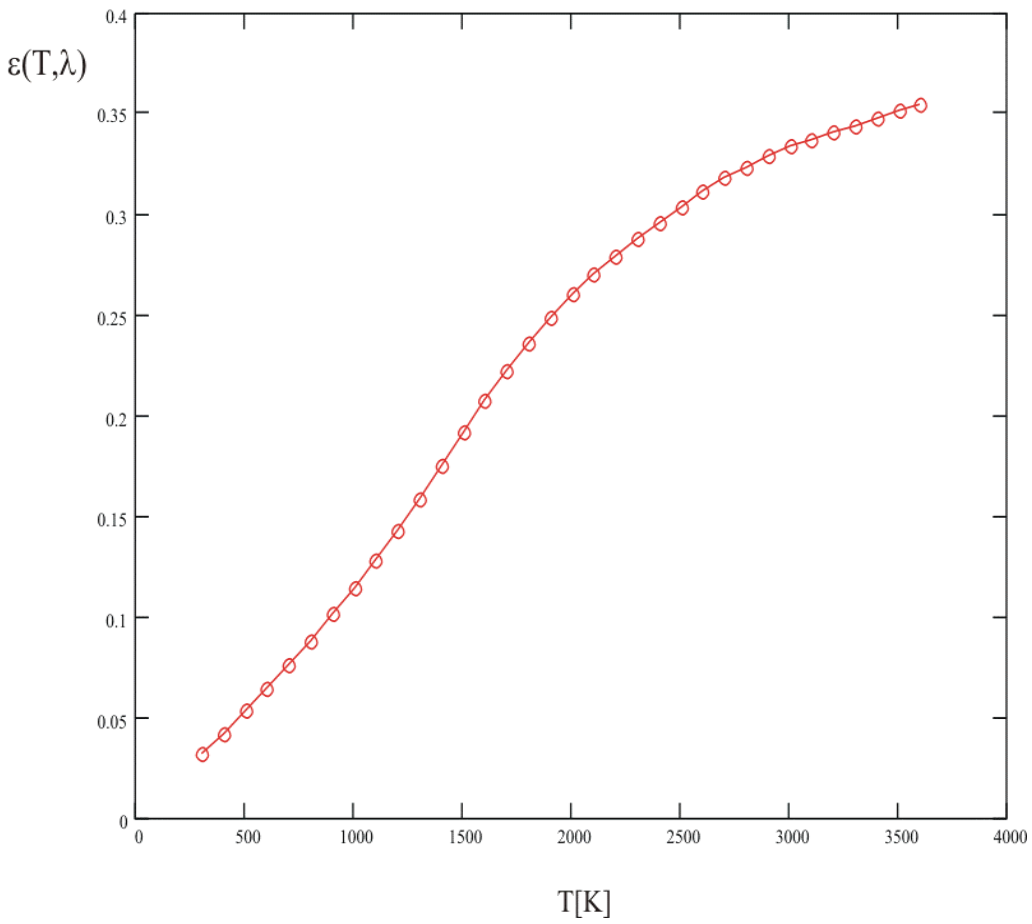

Fig. 4.5 Published tungsten emissivity values increase from 0.05 at room temperature to 0.35 at 3500 K (after Weast, 1970).

Tungsten source emission primarily depends on temperature. At 2800 K, its emissivity for the visible wavelength interval has been measured to be about 0.3, as illustrated in Fig. 4.3. In the same wavelength interval, the change of emissivity with temperature is about 6 x 10^{-5} K^{-1}. For each 10^{M} K of change in temperature, there is 2 x 10^{M-4} change in emissivity, or about 0.02% per K. While this value appears small, it is equal to 2% when dealing with the error in temperature of 100 K. Filament-heating current is kept stable using a regulated power source (see Fig. 4.4).

4.5 Differential two-wavelength thermometry

The radiance of a grey body is given by Planck' law

$$L(T,\lambda) = \varepsilon(T,\lambda)C_1\lambda^{-5}\left[exp\left(c_2/\lambda T\right) - 1\right]^{-1} \quad (4.1)$$

C_1 is different from the first radiation constant ($c_1=2\pi hc^2 = 3.741832x10^{-16}\ Wm^2$) in being smaller than it by a factor π ($C_1 = c_1/\pi$). The second radiation constant c_2 is unchanged ($c_2 = hc/k_B = 1.438786x10^{-2}\ mK$). In the visible region of the electromagnetic spectrum, 1 (one) in the denominator is appreciably smaller than the exponential function and may be neglected, without affecting the accuracy of results (Wien approximation). Then Eq. (4.1) can be simplified :

$$L(T,\lambda) = \varepsilon(T,\lambda)C_1\lambda^{-5}\left[exp\left(-c_2/\lambda T\right)\right] \quad (4.2)$$

Two radiance values are close together because the wavelengths are separated by small value.

$$L_2 = L(T,\lambda_2) = L(T,\lambda_1) + \Delta L(T,\lambda_1) \quad (4.3)$$

For each measurement we obtain the radiance value.

$$L_1 = L(T,\lambda_1) = \varepsilon(T,\lambda_1)C_1\lambda_1^{-5}\left[exp\left(-c_2/\lambda_1 T\right)\right] \quad (4.4)$$

$$L_2 = L(T,\lambda_2) = \varepsilon(T,\lambda_2)C_1\lambda_2^{-5}\left[exp\left(-c_2/\lambda_2 T\right)\right] \quad (4.5)$$

Dividing left and right side of Eq. (4.4) with the corresponding sides in Eq. (4.5), we find,

$$L_1 / L_2 = L(T,\lambda_1) / L(T,\lambda_2) = [\lambda_2 / \lambda_1]^5 \, exp[(-c_2 / T)(1/\lambda_1 - 1/\lambda_2)] \quad (4.6)$$

Here we assumed that the emissivity of the body is the same at both wavelengths. We apply logarithm to the left and right side of Eq. (4.6)

$$ln(L_1 / L_2) = 5\,ln[\lambda_2 / \lambda_1] - (c_2 / T)(1/\lambda_1 - 1/\lambda_2)$$

$$5\,ln[\lambda_2 / \lambda_1] - ln(L_1 / L_2) = (c_2 / T)(1/\lambda_1 - 1/\lambda_2) \quad (4.7)$$

Then the temperature may be found.

$$T = (c_2 / T)(1/\lambda_1 - 1/\lambda_2)[5\,ln[\lambda_2 / \lambda_1] - ln(L_1 / L_2)]^{-1} = T(L(\lambda_2), L(\lambda_1), \lambda_2, \lambda_1) \quad (4.8)$$

This expression is exact in two-wavelength differential thermometry, because the emissivity is the same for both wavelengths. Temperature is obtained upon measuring two radiance values at two distinct wavelengths.

When wavelengths are very close together as in two consecutives spectrometric measurement, differential quantities may be used.

$$\lambda_2 = \lambda_1 + \Delta\lambda_1 \text{ and } \Delta\lambda_1 = \lambda_2 - \lambda_1 \tag{4.9}$$

Emissivity is also a spectral quantity. It is reasonably assumed that its value remains unchanged for two wavelengths, separated by less than 1 nm. Thus, derivative of emissivity with respect to wavelength is zero.

The radiance is a continuous function of wavelength. When the wavelength is changed by small amount, the radiance will be likewise changed by small amount. We make the following simplification, remembering Eq. (4.9) and using binomial expansion for small quantities.

$$\left[\lambda_2 / \lambda_1\right]^5 = \left[1 + \Delta\lambda / \lambda_1\right]^5 =$$
$$1 + 5\Delta\lambda / \lambda_1 + 10(\Delta\lambda / \lambda_1)^2 + 10\left(\Delta\lambda / \lambda_1\right)^3 + 5\left(\Delta\lambda / \lambda_1\right)^4 + \left(\Delta\lambda / \lambda_1\right)^5$$
$$\left[\lambda_2 / \lambda_1\right]^5 = \left[1 + \Delta\lambda / \lambda_1\right]^5 \approx 1 + 5\Delta\lambda / \lambda_1 \tag{4.10}$$

$$1 / \lambda_1 - 1 / \lambda_2 = \Delta\lambda /(\lambda_1\lambda_2) = \Delta\lambda / \lambda^2 \tag{4.11}$$

We replaced the specific subscripts with the running variable to correspond with the spectrometric experiment.

$$L_1 / L_2 = L(T, \lambda_1) / L(T, \lambda_2) = \left[1 + 5\Delta\lambda / \lambda\right] exp\left[\left(-c_2 / \lambda T\right)\left(\Delta\lambda / \lambda\right)\right] \tag{4.12}$$

We take the natural logarithm of the left and right side of Eq. (4.12).

$$ln(L_1 / L_2) = \gamma - \left[\left(c_2\Delta\lambda\right) /(T\lambda^2)\right] \tag{4.13}$$

Here we introduce a constant γ,

$$\gamma = ln(1 + 5\Delta\lambda / \lambda) = 5\, ln(\lambda_2 / \lambda_1)$$

It is a product of 5 and logarithm of the ratio of λ_2 and λ_1, whose value is just slightly larger than zero.

$$ln(L_1 / L_2) - \gamma = -\left[(c_2\Delta\lambda)/(T\lambda^2)\right] \tag{4.14}$$

We can find temperature by solving for T in Eq. (4.14), thus defining differential two-wavelength thermometry:

$$T = (c_2\Delta\lambda) / \left\{\lambda^2\left[ln(L_1 / L_2) - \gamma\right]\right\} \tag{4.15}$$

Substituting the parameter γ again, we obtain:

$$T = (c_2\Delta\lambda) / \left\{\lambda^2\left[ln(L_1 / L_2) - ln(1 + 5\Delta\lambda / \lambda)\right]\right\}$$

$$= T(L(\lambda_2), L(\lambda_1), \lambda_1, \lambda_2) \tag{4.16}$$

Using Eq. (4.10), we attain an expression with single logarithmic function to minimize the manipulation of small quantities.

$$T = \left[(c_2\Delta\lambda) / \lambda^2\right] ln\left[(L_1 / L_2)(\lambda_2 / \lambda_1)^5\right]$$

We note that temperature may be determined if we measured four quantities: two radiances and two specific wavelengths (L_1, L_2, λ_1, λ_2).

4.6 Application to tungsten source

We reported earlier that the temperature of the tungsten filament is not uniform, as assumed previously. We tried to determine the temperature of 0.1-mm^2 area on the tungsten source more accurately, with two-wavelength differential thermometry. Fig. 4.4 shows the temperature as a function of wavelength obtained for a wavelength separation of only 0.3 nm. The measured temperature of the filament is seen to depend on the wavelengths at which the measurements are taken. At 470 nm, its measured value is approximately 2500 K, increasing to about 2950 K at 550 nm. The maximum temperature is reached at 603 nm. We calculated the temperature, T_{avg} = 2869 K, using the complete instrument spectral region from 470 nm to 650 nm. This further variability of results was even more unexpected, prompting us to question the validity of the differential two-wavelength thermometry on a micro scale.

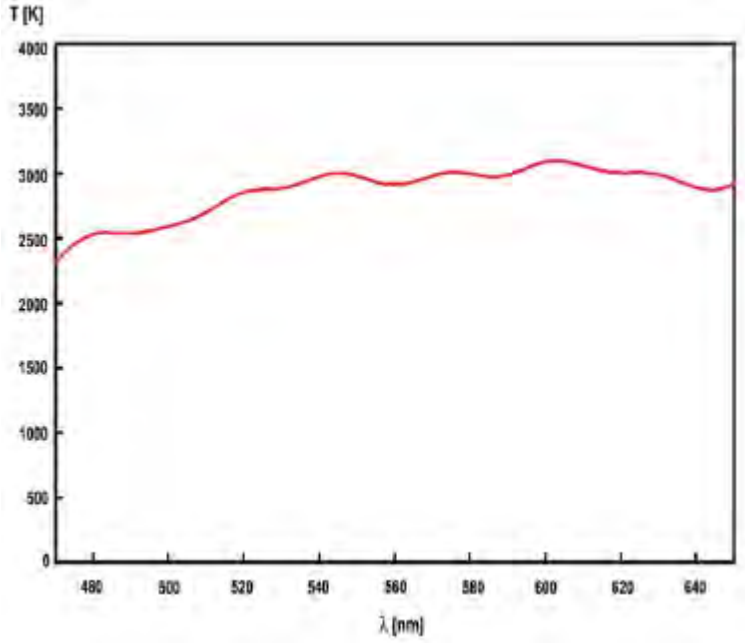

Fig. 4.6 Temperature as a function of monochromator wavelength, measured with differential two-wavelength thermometry. The wavelengths are separated by 0.3 nm to determine temperature of 0.5-mm^2 area on the filament.

4.7 Conclusions

Theoretically, sample temperature may be determined if we measure four quantities (two radiances at two specific wavelengths). Results indicate that differential, continuous thermometry using a spectrometer measures temperature distribution along a short line. This method significantly enhances the capability of this established technique to new applications on a microscopic level. With this measurement we further confirm the establishment of a micro-cavity in tungsten source, and determine temperature of inner and outer coils. We demonstrate that the differential two-wavelength thermometry may provide temperature distribution along a small distance when micro-areas are being imaged on spectrometer entrance pupil. Finally, the challenges of measuring temperatures of micro-surfaces at elevated values remain an area of significant research interest.

References

[1] M.S. Scholl, Temperature calibration of an infrared radiation source, Appl. Opt. 19 (21) (1980) 3622–3625.

[2] M.S. Scholl, Thermal considerations in the design of a dynamic IR target, Appl. Opt. 21 (1982) 660–6671.

[3] J. Castrellon, G. Paez, M. Strojnik, Remote temperature sensor employing erbium-doped silica fiber, Inf. Phys. Tech. 43 (2002) 219–222.

[4] V. Lopez, G. Paez, M. Strojnik, Sensitivity of a temperature sensor, employing ratio of fluorescence power in a band, Inf. Phys. Tech. 45 (2004).

[5] J. Sandoval, G. Paez, M. Strojnik, Er-doped silica dynamic IR-tovisible image converter, Inf. Phys. Tech. 45 (2004).

[6] M.S. Scholl, Errors in radiance simulation and scene discrimination, Appl. Opt. 21 (10) (1982) 1839–1843.

[7] M. Strojnik, G. Paez, Tungsten lamp as radiation standard and the emissivity effects, in: M. Strojnik (Ed.), SPIE Proceedings 5549, Infrared Spaceborne Remote Sensing XII, (2004) 359–367.

[8] G. Paez, M. Strojnik, Cavity effects in coiled coil IR reference source, Inf. Phys. Tech. 49 (2007) 202–204.

Chapter 5

General conclusions

We developed the theoretical expression for the detected thermal contrast detected with the thermal and the quantum detectors in order to perform a reliable comparison and the trade-off analysis between their performance for the routine, remote monitoring of agricultural process. Our analysis includes the contribution to the radiative emission arising from the emissivity change in addition to the traditionally considered one due to temperature change. The empirical rule-of-thumb developed by the long-time practitioner confirms the importance of the second term at room temperature. The additional finding demonstrated in this work is that the contribution due to emissivity changes has been underestimated. It introduces about *30%* error for the detected thermal contrast at room temperature.

We note that under the same conditions the quantum detector measures *20* times higher detected thermal contrast than the thermal one in either spectral interval, independently of the magnitude of the change of emissivity value.

Thus, we conclude that the quantum detector exhibits better performance than thermal detector for the remote monitoring of agricultural crops, especially in the case of the urgent need of the early disease detection.

The factor of improvement in the contrast detected with the quantum detector over that with the thermal detector is also about *20* when the detected thermal contrast arises solely due to the change in emissivity. This is significant in the interesting case that the

infected plant undergoes only emissivity change without the accompanying change in temperature.

The magnitude of the thermal contrast arising solely due to the emissivity term may be determined only when data on emissivity deterioration in-situ, and with use, such as the lifetime data, becomes available.

For the two materials that are important for infrared mirror surface, one may safely conclude that the real change of temperature of *1* K results in a the change of the radiative emission equivalent to temperature change of *1.3* K. Thus neglecting the emissivity term for these materials results in approximately *30%* error.

Theoretically, sample temperature may be determined if we measure four quantities (two radiances at two specific wavelengths). Results indicate that differential, continuous thermometry using a spectrometer measures temperature distribution along a short line. The utility of this method restrict us to an interval of low wavelengths in the visible interval of the electromagnetic spectrum and the error could increase when we dealing with higher temperatures. Also the digitalization process will add an error that could be significant, but in our case we have no such problem using a 12 bits spectrometer. At the microscopic level we further confirm the establishment of a micro-cavity in tungsten source, and determine temperature of inner and outer coils. We demonstrate that the differential two-wavelength thermometry may provide temperature distribution along a small distance when micro-areas are being imaged on spectrometer entrance pupil. Finally, the challenges of measuring temperatures of micro-surfaces at elevated values remain an area of significant research interest.